Sustainable Energy & Fuels



REVIEW

View Article Online
View Journal | View Issue



Cite this: Sustainable Energy Fuels, 2020, 4, 3211

Received 21st March 2020 Accepted 23rd April 2020

DOI: 10.1039/d0se00466a

rsc.li/sustainable-energy

Recent advances of nonprecious and bifunctional electrocatalysts for overall water splitting

Xiao Shang, a Jian-Hong Tang, a Bin Dong to *bc and Yujie Sun to *a

Electrocatalytic water splitting to produce clean hydrogen is a promising technique for renewable energy conversion and storage in the future energy portfolio. Aiming at industrial hydrogen production, cost-effective electrocatalysts are expected to be competent in both hydrogen evolution reactions (HERs) and oxygen evolution reactions (OERs) to accomplish the overall water splitting. Limited by the low tolerance and/or poor activity of most 1st-row transition metal-based electrocatalysts in strongly acidic media, bifunctional electrocatalysts are currently advocated to work at high pH values. Herein, this review summarizes the recent progress of nonprecious bifunctional electrocatalysts for overall water splitting in alkaline media, including transition metal-based phosphides, chalcogenides, oxides, nitrides, carbides, borides, alloys, and metal-free materials. Besides, some prevalent modification strategies to optimize the activities of catalysts are briefly listed. Finally, the perspective on current challenges and future prospects for overall water splitting driven by advanced nonprecious electrocatalysts are briefly discussed.

1. Introduction

Electrocatalytic water splitting to produce clean hydrogen (H₂) has gained intense interest during the last decade, in that H₂ is widely recognized as a green fuel and energy carrier, and it plays an important role in the current chemical industry as well as future energy portfolio. The overall water splitting electrolysis can be divided into two half reactions: the cathodic hydrogen evolution reaction (HER) and the anodic oxygen evolution reaction (OER). Both half reactions involve multi-electron transportation on intermediates, varied by the pH conditions as shown in Fig. 1. The general mechanism of HERs involves an electrochemical hydrogen adsorption step followed by an electrochemical desorption or recombination reaction. In the case of OERs, it involves the formation of adsorbed OH* on the catalyst surface with the subsequent transformation to OOH* and the eventual release of O2.2 The standard thermodynamic voltage to split water is 1.23 V, whereas a higher voltage is actually required in practical circumstances. The extra overpotentials mainly come from the devices and intrinsic activation barriers of electrodes.3 The electrode also involves slow reaction kinetics such as reactants adsorption/desorption, electric contact, and gas-involving interface that limit the hydrogen production rate.3 Therefore, the practical water

The above-discussed situation necessitates active electrocatalysts to simultaneously reduce the operation overpotential and enhance the reaction speed. To date, noble metals (platinum groups) and noble oxides (Ru or Ir oxides) are demonstrated as the most active HER and OER electrocatalysts, respectively.^{3,4} However, their scarcity and high cost are major obstacles in the large-scale water splitting. Therefore, tremendous efforts are focused on exploiting inexpensive alternatives such as transition metal-based and metal-free materials.

In order to be economically attractive, it is preferred to conduct both half reactions of water splitting in the same electrolyte. If an electrocatalyst is active for both half HERs and OERs in the same electrolyte, then it will further simplify the manufacture of a water splitting electrolyzer. Given the severe corrosion and/or poor activity of most 1st-row transition metalbased electrocatalysts for OERs in strongly acidic electrolytes,

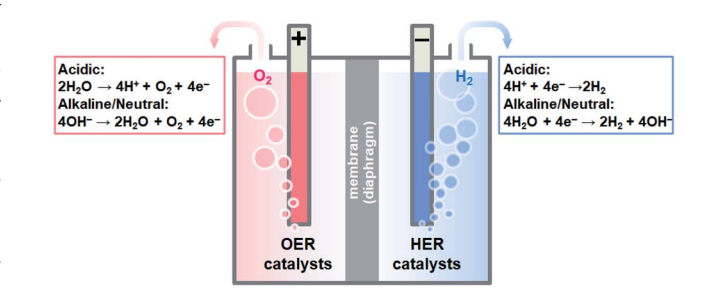


Fig. 1 Scheme of a conventional water electrolyzer with two half reactions under acidic and alkaline/neutral conditions.

electrolysis confronts both electrode thermodynamic and kinetic issues.

[&]quot;Department of Chemistry, University of Cincinnati, Cincinnati, OH 45221, USA. E-mail: yujie.sun@uc.edu

bState Key Laboratory of Heavy Oil Processing, China University of Petroleum (East China), Qingdao 266580, PR China. E-mail: dongbin@upc.edu.cn

^cCollege of Science, China University of Petroleum (East China), Qingdao 266580, PR China

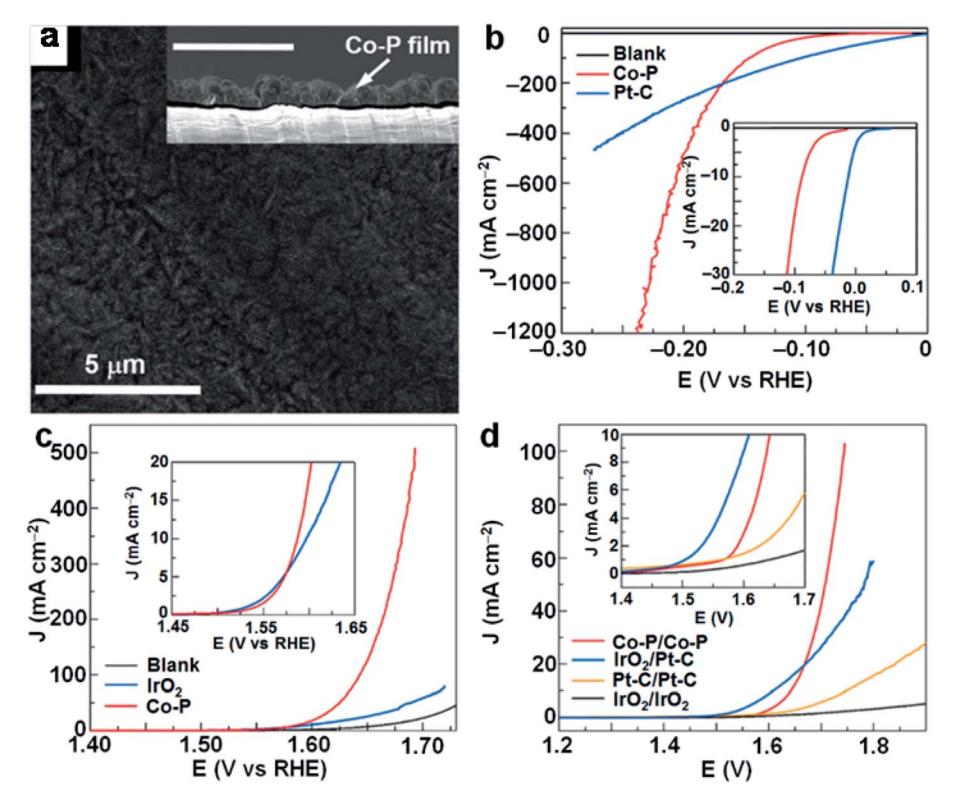


Fig. 2 (a) SEM image of electrodeposited Co-P film (inset: cross section SEM image). LSV curves of Co-P, Pt-C and blank Cu foil for HERs (b), OERs (c), and overall water splitting (d) in 1.0 M KOH (insets: expanded LSV onset regions). Reproduced from ref. 14. Copyright 2015 John Wiley & Sons. Inc.

there is a growing interest in developing so-called bifunctional electrocatalysts for overall water splitting at high pH. Herein, we summarize the recent advances of nonprecious electrocatalysts for overall water splitting with a particular emphasis on alkaline electrolytes. Several representative catalyst categories including transition metal-based phosphides, chalcogenides, oxides, nitrides, carbides, borides, alloys, and even metal-free materials are highlighted. Several designing strategies for improving activities are also discussed with the aim of providing guidance in designing new electrocatalysts. Finally, our perspective on the current challenges and future opportunities of water splitting driven by low-cost and competent electrocatalysts are included.

phosphide electrocatalysts can be generally grouped into three main categories: mono metal phosphides, binary metal phosphides, and ternary metal phosphides.

Mono metal phosphides such as Co-P, Ni-P, Fe-P, Mo-P, and Cu-P have been widely used as efficient bifunctional electrocatalysts for overall water splitting due to the facile preparation method, earth-abundant material, and outstanding performance. Transition metal-based phosphides (TMPs) have long been utilized as hydroprocessing catalysts in chemical industries.6 A notable example is Ni2P, which was first theoretically predicted and later experimentally proved to be capable of

Representative nonprecious and bifunctional electrocatalysts

2.1 Transition metal-based phosphides

Benefiting from high conductivity, metallic character, and the electronegativity of P sites to trap protons,5 transition metalbased phosphides have recently emerged as promising nonprecious alternatives to noble metals and oxide-based electrocatalysts for overall water splitting. To date, a large number of transition metal-based phosphide electrocatalysts have been developed using the strategies of phosphorization, metaldoping and theoretical calculations. According to the number of metal elements, the reported transition metal-based

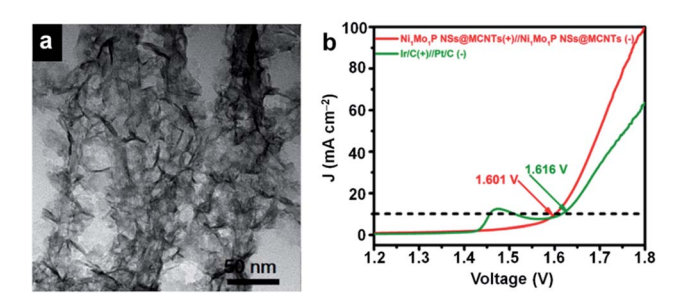


Fig. 3 (a) TEM image of Ni₁Mo₁P NSs@MCNTs. (b) LSV curves of Ni_1Mo_1P NSs@MCNTs(+)//Ni₁Mo₁P NSs@MCNTs(-) and Ir/C(+)//Pt/ C(-) catalyst couples for overall water splitting. Electrolyte: 1.0 M KOH; scan rate: 5 mV s⁻¹. Reproduced from ref. 16. Copyright 2018, American Chemical Society.

catalyzing HERs.^{7,8} Subsequently, many TMPs including those based on Co, Fe and Cu have been explored as promising HER electrocatalysts.9-13 For instance, Sun et al. investigated the electrodeposited Co-P films as the bifunctional electrocatalysts for both HERs and OERs under alkaline conditions.14 Using CoSO₄ and NaH₂PO₂ as the Co and P sources, respectively, amorphous Co-P films were prepared by a potentiodynamic deposition method (Fig. 2a). Linear sweep voltammetry (LSV) of Co-P exhibited a HER catalytic onset potential of -50 mV *versus* reversible hydrogen electrode (vs. RHE), as shown in Fig. 2b. Even though its onset potential was slightly more negative than that of Pt-C, the behaviors of Co-P surpassed Pt-C beyond −167 mV vs. RHE (Fig. 2b). Moreover, Co-P materials could also

be directly applied for OERs. As shown in Fig. 2c, Co-P produced a current density of 10 mA cm⁻² at an overpotential of 345 mV and rivaled the performance of IrO2 as measured under the same OER condition. Post electrocatalysis characterization revealed that the in situ formed cobalt oxides and (oxy)hydroxides were most likely the real OER active species on Co-P. When Co-P was utilized as an electrocatalyst for both cathodes and anodes, it only required a voltage of 1.744 V to deliver 100 mA cm⁻² in a two-electrode configuration (Fig. 2d). Recently, Hu et al. have reported a Ni₂P-based Janus electrocatalyst for overall water splitting, which generated 10 mA cm⁻² at 1.63 V while serving as both cathode and anode catalysts under alkaline conditions.15

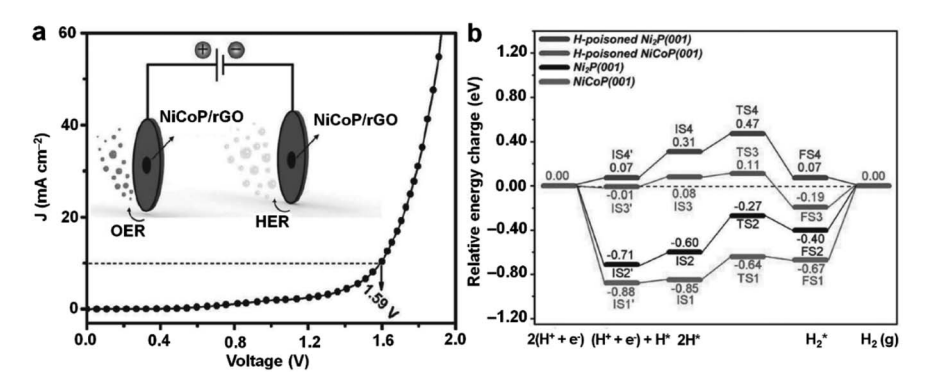


Fig. 4 (a) LSV curve of NiCoP/rGO for overall water splitting in 1.0 M KOH at a scan rate of 5 mV s $^{-1}$. Inset shows the schematic overall water splitting in a two-electrode configuration. (b) Calculated energy profiles for HERs on pristine and H-poisoned NiCoP (0001) and Ni₂P (001) facets. The relative energies are plotted with respect to the energy change in the reaction of $2(H^+ + e^-) \rightarrow H_2$. Reproduced from ref. 22. Copyright 2016 John Wiley & Sons, Inc.

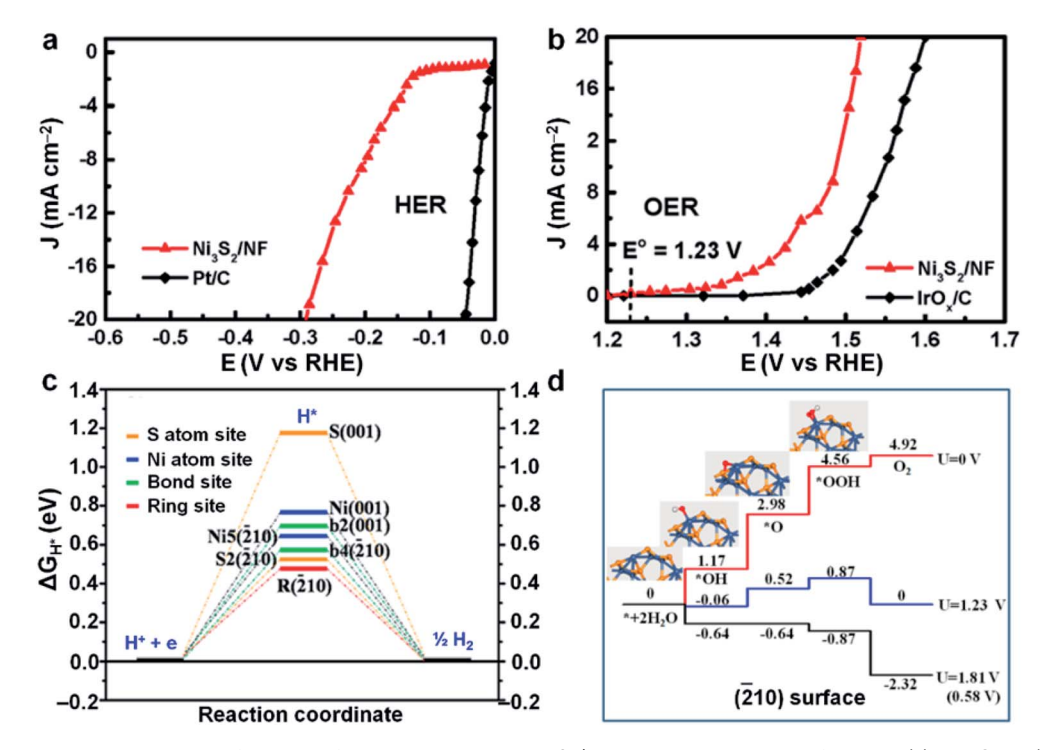


Fig. 5 Steady-state current density as a function of applied voltage on Ni₃S₂/NF and control samples for HERs (a) and OERs (b) in 1.0 M NaOH. Calculated free energy diagram on Ni₃S₂ for HERs (c) and OERs (d). Reproduced from ref. 35. Copyright 2015 American Chemical Society.

In order to enhance the intrinsic activity of mono metal phosphide materials, an extrinsic metal-doping methodology has been well developed for fabricating efficient binary metal phosphide and ternary metal phosphide water splitting electrocatalysts. ¹⁶⁻²¹ For example, Du *et al.* introduced molybdenum into nickel phosphide nanosheets on carbon nanotubes (Ni₁Mo₁P NSs@MCNTs, as shown in Fig. 3a). ¹⁶ The reported binary metal phosphides exhibited excellent overall water splitting performance with a low cell voltage of 1.601 V to drive 10 mA cm⁻² (Fig. 3b). The abundant micropores and defects in

the hierarchical structure of Ni_1Mo_1P NSs@MCNTs were proposed to provide the active sites and facilitate mass/ion diffusion. A series of Co-doped nickel phosphide (NiCoP) bifunctional catalysts were reported by Qu, Ma, Chang and co-workers. As shown in Fig. 4a, the NiCoP hybrids on reduced graphene oxides showed a catalytic current density of 10 mA cm $^{-2}$ at 1.59 V for overall water splitting. Combining electrochemical measurements with density functional theory (DFT) calculations (Fig. 4b), it was revealed that Co-doping modulated the surface active sites, accelerated the charge

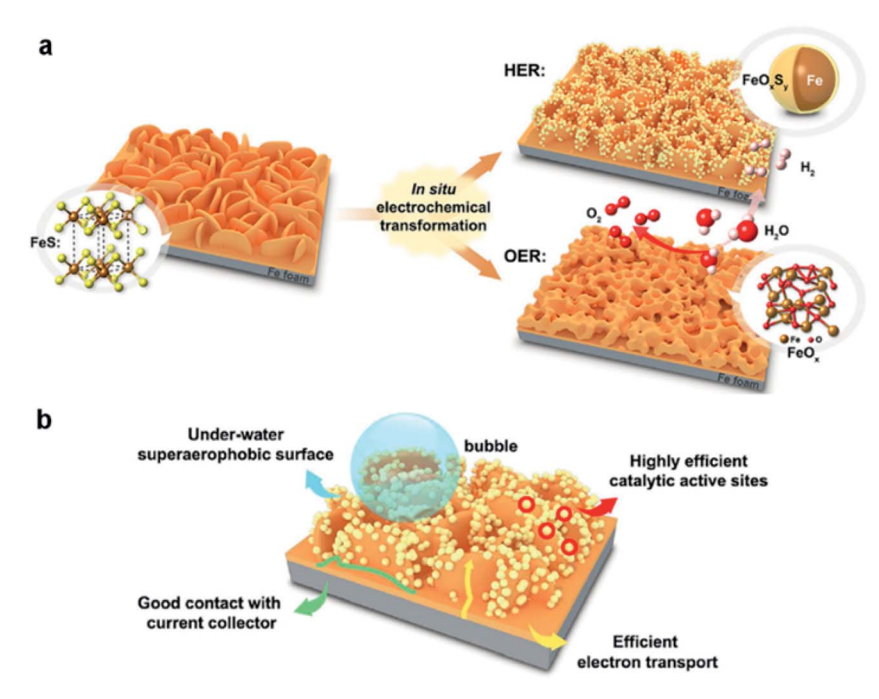


Fig. 6 (a) Scheme of the *in situ* transforming FeS/IF pre-catalyst into Fe $-H_2$ cat for HERs and Fe $-O_2$ cat for OERs. (b) Scheme of several key factors contributed to the highly active Fe $-H_2$ cat. Reproduced from ref. 28 Copyright 2018 Elsevier.

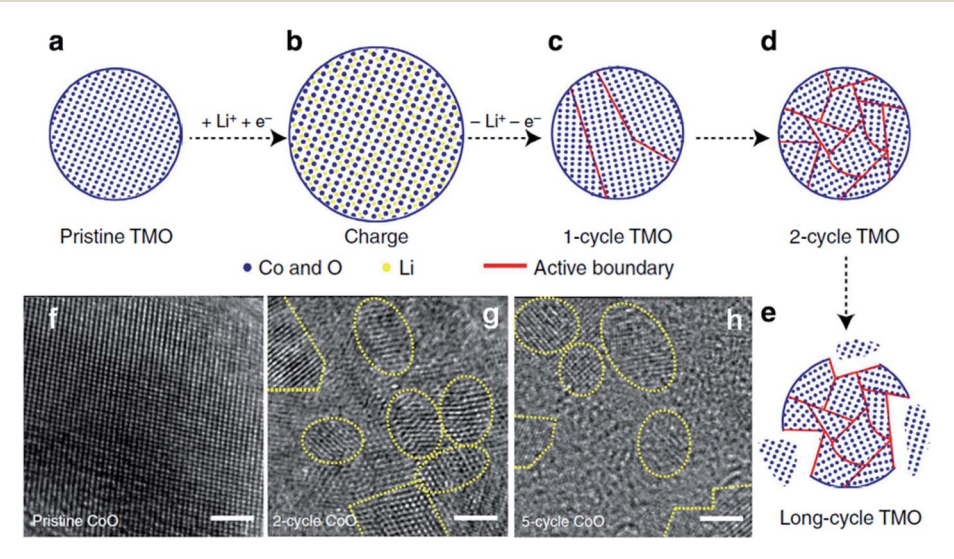


Fig. 7 (a–e) Schematic of the morphological evolution of TMO under galvanostatic cycles. The TMO particles gradually change from single crystalline to ultra-small interconnected crystalline nanoparticles. HRTEM images of (f) pristine, (g) 2-cycle, and (h) 5-cycle carbon nanofiber-supported CoO (CoO/CNF). Scale bar: 2 nm. Reproduced from ref. 40. Copyright 2015 Nature Publishing Group.

transfer, and boosted their superior catalytic activity. Subsequently, Tang et al. developed a Ni-Co-Cu ternary metal phosphide heterostructure (NiCoP@Cu₃P) for water splitting. Due to the multiple synergistic effects of the ternary catalyst, it exhibited an enhanced catalytic performance for both HERs and OERs in an alkaline solution.23

Transition metal-based chalcogenides

Transition metal-based chalcogenides including sulfides and selenides have attracted considerable attention for enhanced electrocatalytic HER and OER applications owing to their rich electrochemical properties.24 By hybridizing with the nonprecious transition metals such as Ni, Co, Fe, and alloys,25-34 a variety of transition metal-based chalcogenide electrocatalysts have been explored for overall water-splitting.

In 2015, Zou et al. synthesized Ni₃S₂ nanosheet arrays on a nickel foam (NF) via direct hydrothermal sulfurization of NF using thiourea as a source of sulfur (denoted Ni₃S₂/NF).³⁵ The resultant Ni₃S₂/NF delivered a current density of 10 mA cm⁻² at quite low overpotentials of 223 and 260 mV for HERs (Fig. 5a) and OERs (Fig. 5b), respectively. DFT computations revealed that the exposed high-index facets of Ni₃S₂ decreased the coordination number of Ni and S sites and lowered the free energy of intermediate H* adsorption (ΔG_{H^*}), which was

beneficial to the overall HER performance (Fig. 5c). Meanwhile, the energy barriers for critical OER steps were also decreased (Fig. 5d). By electrochemical desulfurization of iron sulfide supported on iron foam, Zhang et al. reported FeS/IF electrocatalysts for high-performance alkaline overall water splitting (Fig. 6a).28 The high catalytic activity of FeS/IF was attributed to the following advantages (Fig. 6b): (i) the self-supported, hierarchical, and metallic scaffold (FeS/IF) rendered abundant active site on the catalyst surface and excellent conductivity; (ii) the superaerophobicity of Fe@FeO_xS_v promoted mass diffusion at the multi-phase interfaces; and (iii) the higher intrinsic activity of Fe@FeO_xS_v was the most important factor for HERs and enhanced the overall water splitting performance.

In addition to the above-mentioned examples, Sun et al. reported in situ growth of NiSe nanowires on NF (NiSe/NF) under hydrothermal conditions. The as-prepared 3D NiSe/NF electrocatalysts exhibited high catalytic activity and durability for both OERs and HERs under alkaline conditions. In a two-electrode configuration, this bifunctional alkaline water electrolyzer enabled 10 mA cm⁻² under a cell voltage of 1.63 V. They proposed that the NiOOH species formed at the NiSe surface acted as the actual catalytic site.32 Recently, Driess et al. have prepared a highly active FeSe2 electrocatalyst for durable overall water splitting.36 The formation of Fe(OH)2/FeOOH active sites

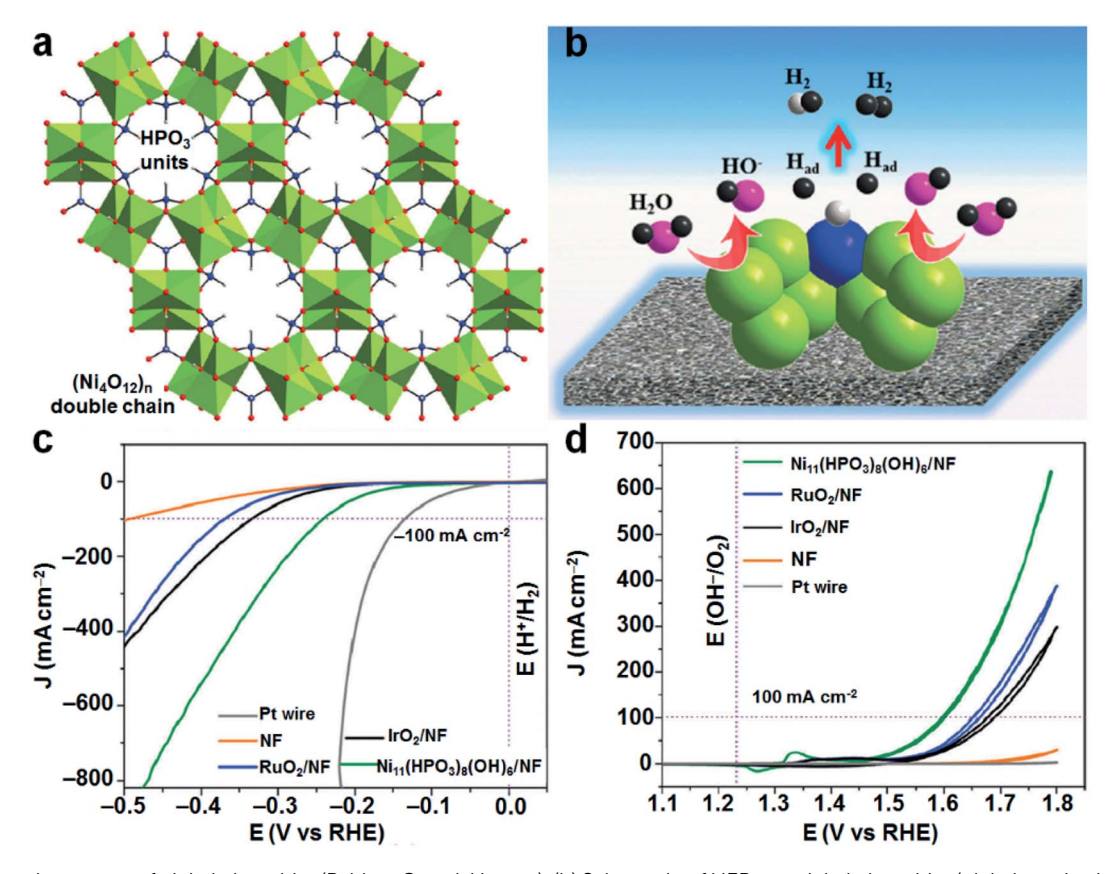


Fig. 8 (a) Crystal structure of nickel phosphite (P: blue, O: red, H: grey). (b) Schematic of HERs on nickel phosphite (nickel octahedral: chartreuse, phosphite: blue, H: grey). Electrocatalytic performances of nickel phosphite supported on Ni foam (NF) compared with noble metal-based catalysts in 1.0 M KOH: (c) LSV curves for HERs (scan rate: 5 mV s⁻¹) and (d) cyclic voltammogram plots for OERs (scan rate: 1 mV s⁻¹). Reproduced from ref. 58. Copyright 2018 The Royal Society of Chemistry.

and defect structure with anionic vacancies contributed to the outstanding catalytic activity and stability, exhibiting a low overpotential (245 mV) at 10 mA cm $^{-2}$ for OERs. Liu *et al.* synthesized monoclinic $\rm Co_3Se_4$ thin nanowires on cobalt foam (Co $_3Se_4$ /CF), which could deliver 10 and 20 mA cm $^{-2}$ at low cell voltages of 1.59 and 1.63 V using an electrolyzer. 31

2.3 Transition metal-based oxides

Because of their low cost, high intrinsic activity, and robust stability, transition metal-based oxides (TMOs) have provided a promising possibility in developing bifunctional catalysts with efficient electrocatalytic activities.^{37–39} For instance, Cui and coworkers reported an unconventional top-down electrochemical lithiation method to prepare ultra-small-diameter transition metal-based oxide (iron, cobalt, nickel oxides and their mixed oxides) nanoparticles on carbon nanofibers (Fig. 7a–e).⁴⁰ As

shown in HRTEM images (Fig. 7f–g), CoO-based TMO nanoparticles gradually changed from single crystalline nanoparticles (\sim 20 nm) to interconnected crystalline fragments (2–5 nm). The grain boundaries of the interconnected TMO nanoparticles created additional active sites and also ensured strong interconnection, which maintained good contacts and increased the catalytic activity. In bifunctional water-splitting experiments, the NiFeO_x nanoparticles produced a current density of 10 mA cm⁻² at only 1.51 V, surpassing the IrO₂/Pt couple in 1.0 M KOH. It is worth noting that a large number of electrochemical lithiation cycles may break off the particles and lead to negative effects on the catalytic performance of TMOs (Fig. 7h).

The ABO₃-type perovskite materials have emerged as a new category of efficient TMO electrocatalysts for overall water splitting, due to their intriguing chemical, physical, and catalytic properties. In 2011, Shao-Horn *et al.* reported the

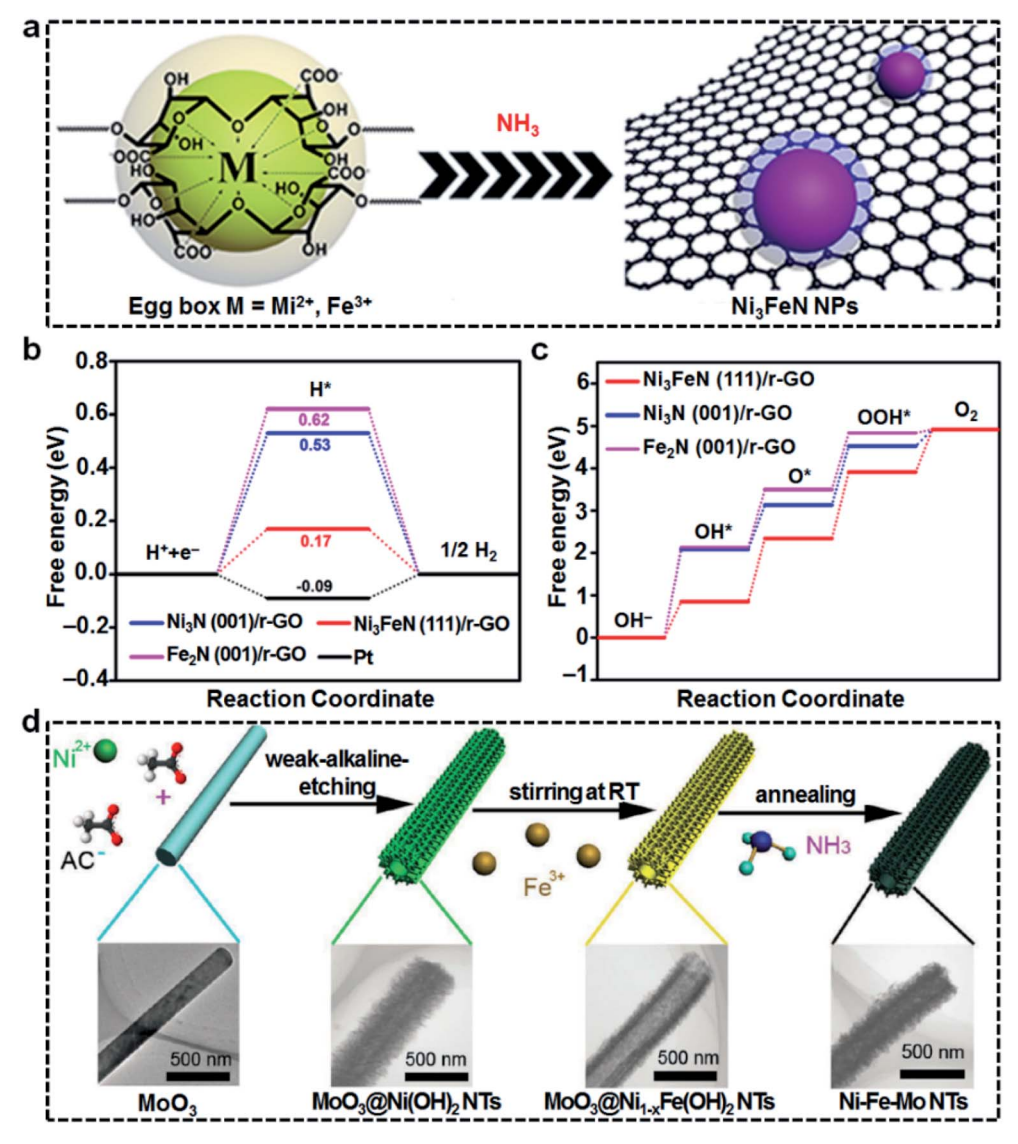


Fig. 9 (a) Schematic of the synthesis of Ni_3 FeN/r-GO derived from sodium alginate with r-GO hydrogels. Schematic free energy profiles for (b) OERs and (c) HERs. (d) Schematic of the synthesis of Ni_7 Fe-Mo nitride nanotubes. (a-c) Reproduced from ref. 70. Copyright 2018 American Chemical Society. (d) Reproduced from ref. 71. Copyright 2018 John Wiley & Sons, Inc.

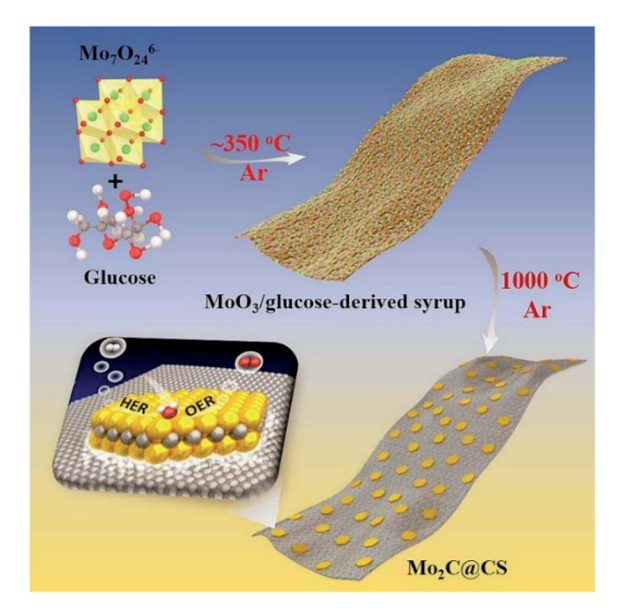


Fig. 10 Schematic of the synthesis of Mo₂C@CS. Reproduced from ref. 87. Copyright 2017 John Wiley & Sons, Inc.

Ba_{0.5}Sr_{0.5}Co_{0.8}Fe_{0.2}O_{3-δ} perovskite electrocatalysts exhibiting a higher OER activity than the state-of-the-art iridium oxide in alkaline media.43 This work stimulated further efforts to optimize the electronic structures of perovskites for developing bifunctional water electrolysis materials.44-46 For instance, Ciucci and co-workers prepared a double perovskite oxide (NdBaMn₂O_{5,5}) with a better overall water splitting activity at large potentials (>1.75 V) and catalytic durability relative to

those of Pt/C-RuO2.44 The outstanding catalytic performance was rationalized by the e_o orbit occupancy, optimized O p-band center location, and distorted structure.

Transition metal-based hydroxides/(oxy)hydroxides, as analogous to transition metal-based oxides, have also been demonstrated for efficient bifunctional overall water splitting,47,48 such as Ni(OH)2,49 VOOH,50 FeOOH,51 and many bimetallic hydroxides. 52-55 The metal original oxyhydroxides species or in situ formed metal oxyhydroxides from pristine catalysts were regarded as real active species for OERs,56 and they were also active for HERs by facilitating water dissociation as a rate-limiting step.57 In 2018, Driess reported a nickel phosphate (Ni₁₁(HPO₃)₈(OH)₆) bifunctional electrocatalyst with remarkable activity and excellent stability both on nickel foam (NF) and on fluorine doped tin oxide in alkaline media (Fig. 8a).58 In situ and ex situ spectroscopic techniques were employed to characterize the formation of nickel oxyhydroxide active sites for both OER and HER half-reactions (Fig. 8b). As shown in Fig. 8c, Ni₁₁(HPO₃)₈(OH)₆ catalysts required a low overpotential of 121 mV to reach 10 mA cm⁻² at the cathode, comparable to that of Pt catalysts. At the anode, it delivered 10 mA cm⁻² at an overpotential of 232 mV and surpassed those of noble RuO2 and IrO2 catalysts (Fig. 8d). While used as an overall water splitting bifunctional electrocatalyst, it showed a low cell voltage of 1.6 V at 10 mA cm^{-2} in alkaline media.

Transition metal-based nitrides

Transition metal-based nitrides (TMNs) are interstitial compounds where nitrogen atoms are integrated into interstitial sites. The electronic redistributions of TMNs improve the

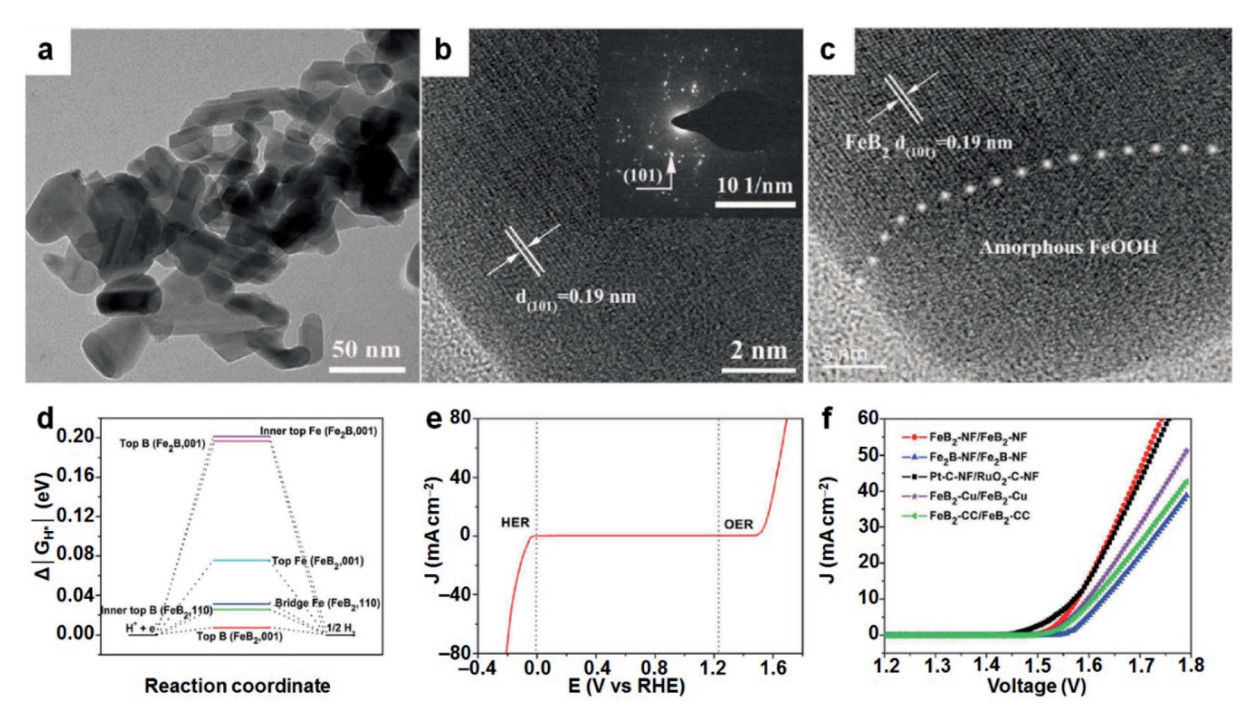


Fig. 11 (a and b) TEM images of FeB₂. (c) HRTEM image of FeB₂ after OERs for 12 h. (d) Calculated free energy diagram of HERs on the (001) and (110) facets of FeB2 and Fe2B at equilibrium potential. (e) LSV curves for HERs and OERs in a three-electrode configuration. (f) LSV curves of overall water splitting in a two-electrode configuration. Reproduced from ref. 91. Copyright 2017 John Wiley & Sons, Inc.

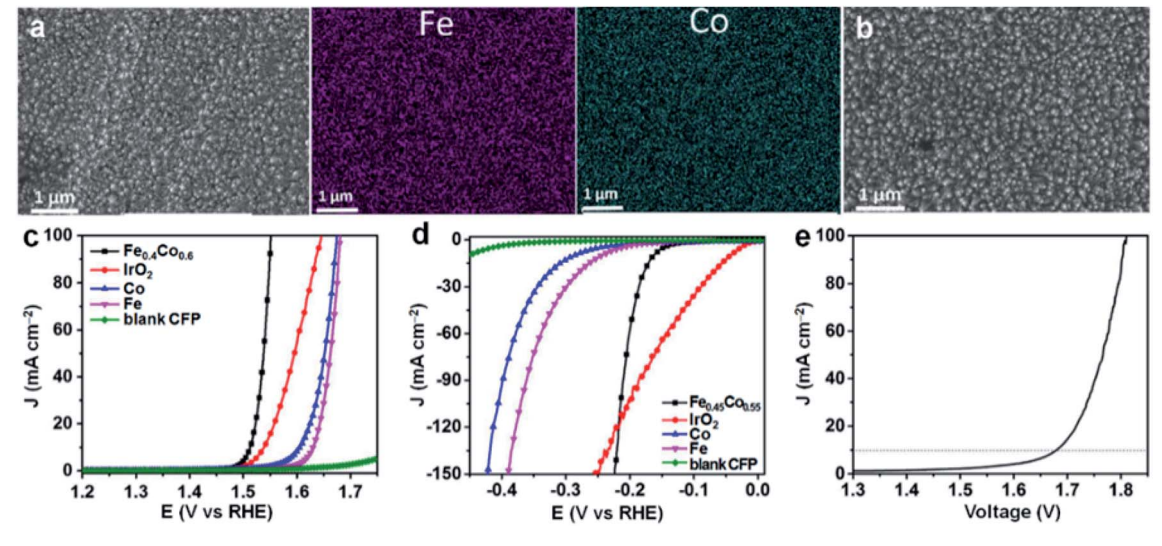


Fig. 12 (a) SEM image with elemental mapping of Fe_{0.4}Co_{0.6} composite films for OERs. (b) SEM image of Fe_{0.4}Co_{0.6} composite films for HERs. LSV curves of OERs (c), HERs (d), and overall water splitting (e) in 1.0 M KOH. Scan rate: 1 mV s⁻¹. Reproduced from ref. 99. Copyright 2017

conductivity, catalytic efficiency, and long-term stability. 59,60 A number of TMNs have been prepared by a nitridation method via tuning the structural and electronic environment around the metal centers, 61,62 such as nickel nitride, 63,64 Co-V nitride, 65 Ni-Mo nitride, 66,67 Ti-N, 68 and Ni-Fe nitride. 69 In 2015, Shalom et al. reported a nickel nitride electrocatalyst for both HERs and OERs by growing nickel nitrides (Ni₃N) on a Ni-foam.⁶⁴ The increase of active Ni²⁺ species and in situ formation of Ni hydroxides led to its enhanced electrocatalytic activity for water splitting. By encapsulating the Ni-Fe nitrides in reduced graphene oxides, Yao et al. developed a bimetallic Ni₃FeN/r-GO catalyst by a one-step nitridation process with alginate hydrogels (Fig. 9a).70 The as-prepared Ni₃FeN/r-GO alkaline electrolyzer could generate 10 mA cm⁻² at 1.60 V with long durability. Theoretical calculations revealed that the reduced ΔG_{H^*} on Ni₃FeN(111) and the redistributed charge at interfaces between Ni₃FeN and r-GO contributed to high HER activity (Fig. 9b). The optimized binding energies on Ni₃FeN benefited to the enhanced OER activity (Fig. 9c). Recently, a multi-step synthetic strategy has been reported by Chou et al. for fabricating hierarchical Ni-Fe-Mo tri-metal nitrides via room-temperature Fe incorporation and NH₃ thermal treatment (Fig. 9d).⁷¹ The prepared Ni-Fe-Mo catalysts drove 10 mA cm⁻² at 1.513 V in a two-electrode cell, outperforming most of the reported bifunctional catalysts.

2.5 Transition metal-based carbides

Transition metal-based carbides (TMCs) display similar electronic and catalytic properties to Pt-group metals, which

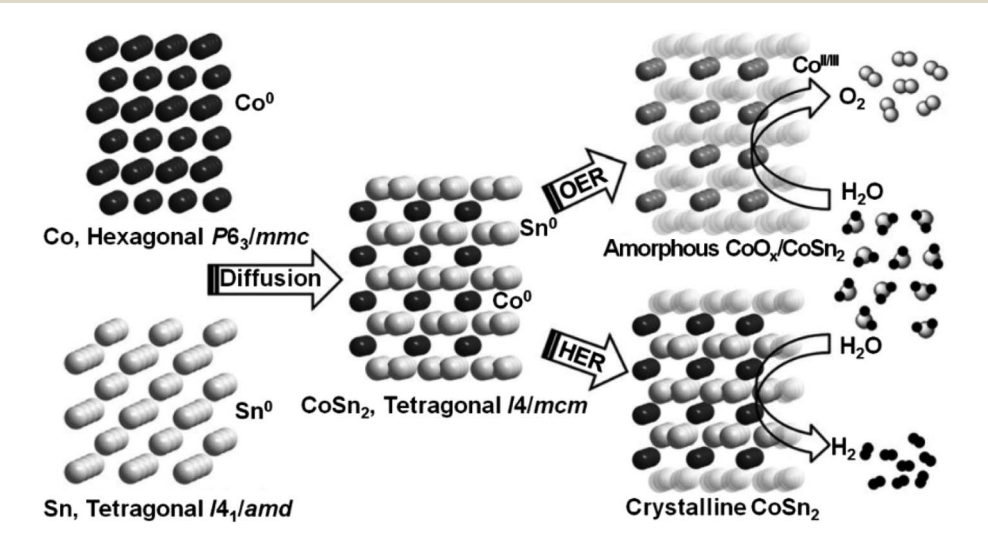


Fig. 13 Unit cell structures of Co (black), Sn (light gray), and CoSn₂ (mixed black and light gray) and the structural modification of CoSn₂ during OERs and HERs in strongly alkaline media. Reproduced from ref. 100. Copyright 2018 John Wiley & Sons, Inc.

have been actively reported as promising electrocatalysts for HER and OER applications. 72-81 Generally, chemical/physical vapor deposition (CVD), electrochemical deposition and pyrolysis of metal complexes are mainly three kinds of methods to prepare TMCs such as Mo, W, Fe, Ni carbides.82-86 Gao et al. synthesized a Mo2C bifunctional electrocatalyst supported on carbon sheets (Mo₂C@CS) by a one-pot pyrolysis process of glucose and ammonium molybdate (Fig. 10).87 Benefitting from the synergistic effects between Mo₂C and carbon sheets, the Mo₂C@CS catalyst exhibited superior activities for both HERs and OERs. In order to improve the relatively weak OER activities of metal carbides, the strategy of inducing other species such as Co86 and NiFe alloys88 has been developed as an effective way to enhance the overall water splitting performance. For instance, Lin and co-workers prepared MoC2-doped NiFe alloy nanoparticles by a one-step calcination process.88 The hybrid bifunctional electrocatalysts achieved an overall water-splitting current density of 10 mA cm⁻² at a low potential of 1.53 V in alkaline media, surpassing the precious Pt/C//RuO2 counterpart.

Transition metal-based borides

Transition metal-based borides are intermetallic compounds with electron-deficient boron elements. The low electronegativity characteristic of boron allows transition metal-based borides to present unusual structural and chemical properties.89 The presence of boron is capable of reducing the hydroxylation reaction barrier, which stimulates the research efforts to explore the transition metal-based boride electrocatalysts for overall water splitting.90-95 In particular, both amorphous and crystalline transition metal-based borides have been reported as efficient bifunctional catalysts for both the HER and OER. For instance, Schuhmann et al. reported amorphous cobalt boride (Co₂B) electrocatalysts using the chemical reduction of CoCl2 with NaBH4.90 During water electrolysis in a two-electrode cell, the optimized Co2B achieved a current density of 10 mA cm⁻² at 1.61 V on an inert support and at 1.59 V when impregnated with nitrogen-doped graphenes. Geyer and co-workers prepared crystalline boride-rich FeB2 nanoparticles by chemical reduction of Fe2+ using LiBH4 (Fig. 11a).91 For the OER, the formation of the FeOOH/FeB2 heterojunction facilitated its catalytic activity (Fig. 11b and c).

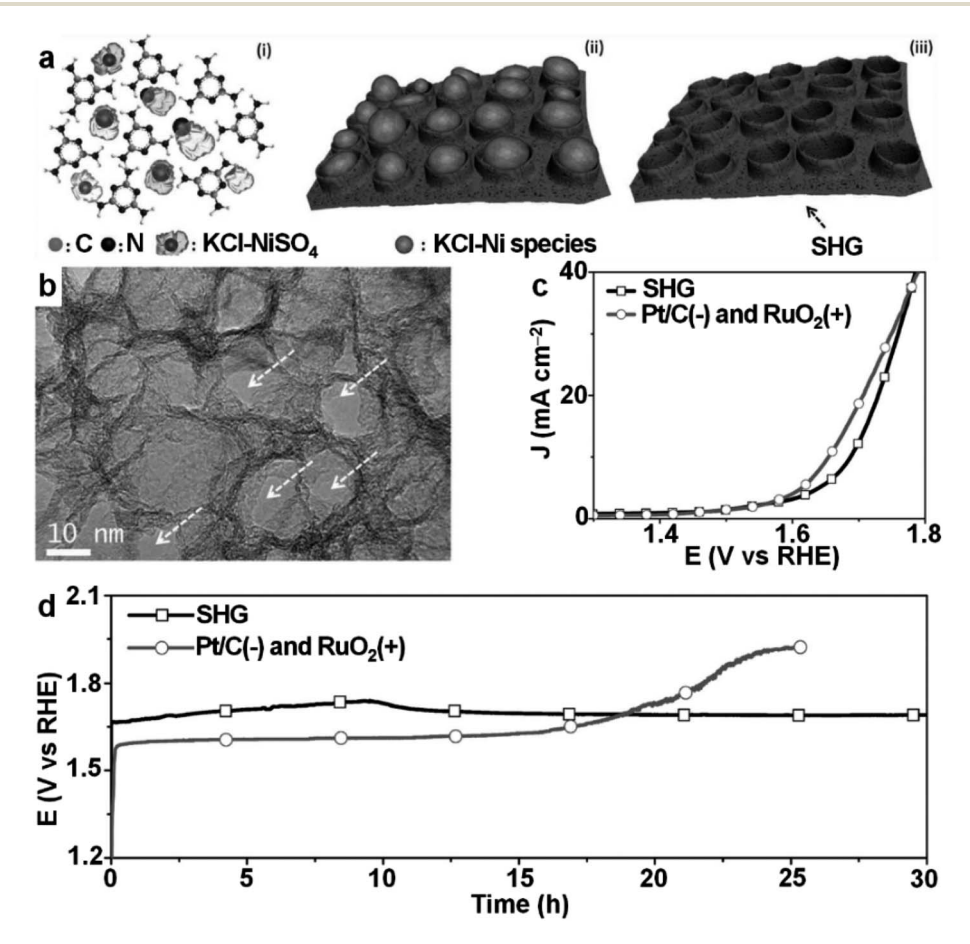


Fig. 14 (a) Schematic of the synthesis of N, S co-doped graphitic sheets (SHG): (i) mixture of melamine, nickel sulfate, and KCl formed by ball milling; (ii) in situ growth of Ni-KCl@SHG; (iii) formation of SHG by etching the Ni@KCl and KCl seeds. (b) TEM image of SHG. (c) LSV curves of SHG and Pt/C-RuO₂ catalyst couples for overall water splitting in 1.0 M KOH at a scan rate of 10 mV s⁻¹. (d) Chronopotentiometric curves of overall water splitting electrolysis catalyzed by SHG and $Pt/C-RuO_2$ couples with a constant current density of 10 mA cm⁻² in 1.0 M KOH. Reproduced from ref. 106. Copyright 2017 John Wiley & Sons, Inc.

Theoretical calculations revealed that the boron-rich surface regulates the binding energy for chemisorption and desorption of hydrogen-containing intermediates, enhancing the HER performance (Fig. 11d, e). In overall water splitting experiments, the FeB₂ electrolyzer delivered a current density of 10 mA cm $^{-2}$ at a low cell voltage of 1.57 V (Fig. 11f).

2.7 Transition metal alloys

Transition metal alloys comprising two or more metallic elements possess many intriguing advantages of unusual and attractive crystallographic and electronic properties for heterogeneous water splitting catalysis. ^{96–98} For instance, Li *et al.* prepared Fe–Co alloy films on carbon fiber papers by one-step electroreductive deposition (Fig. 12a and b). ⁹⁹ By tuning the

ratio of precursor metals, the optimized $Fe_{0.4}Co_{0.6}$ film exhibited excellent OER activity with a low overpotential of 283 mV at $10~\text{mA}~\text{cm}^{-2}$, which was better than that achieved with precious IrO_2 catalysts (Fig. 12c). Another $Fe_{0.45}Co_{0.55}$ film displayed high HER activities showing an overpotential of 163 mV at 10 mA cm $^{-2}$ (Fig. 12d). During use as bifunctional catalysts for overall water splitting, $Fe_{0.45}Co_{0.55}$ composite films exhibited a low voltage of 1.68 V at 10 mA cm $^{-2}$ (Fig. 12e). The *in situ* generated metallic hydroxides/oxides and the metals are beneficial for efficient OERs and HERs, respectively. Very recently, Driess and co-workers synthesized the atomically ordered intermetallic $CoSn_2$ nanocrystals using a solution chemistry method, which showed excellent catalytic activity and long-term stability for OERs, HERs, and overall water-splitting in alkaline media

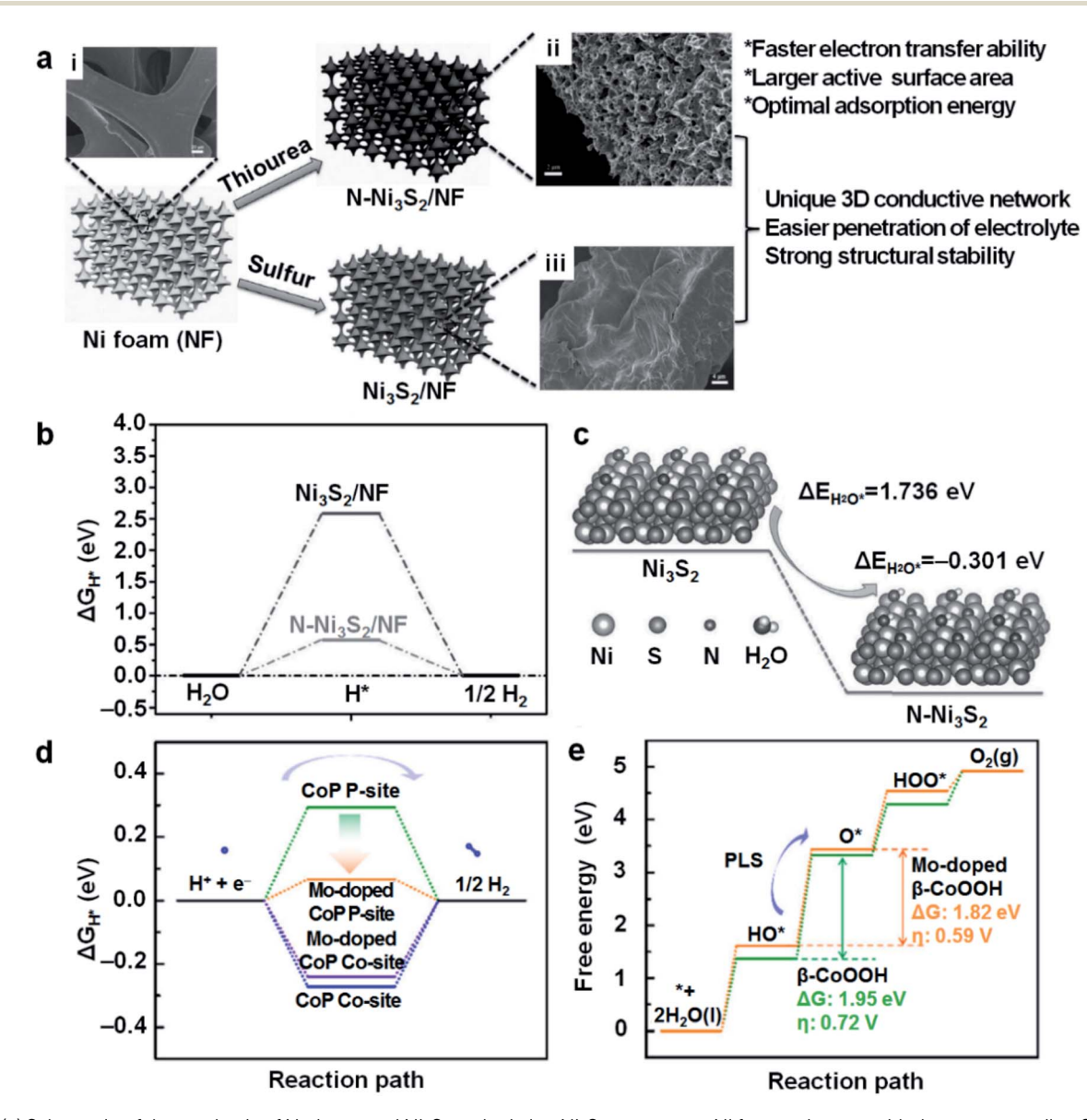


Fig. 15 (a) Schematic of the synthesis of N-decorated Ni_3S_2 and pristine Ni_3S_2 grown on a Ni foam substrate with the corresponding SEM images of NF (i), N-Ni $_3S_2$ /NF (ii), and Ni_3S_2 /NF (iii). Calculated hydrogen (b) and water (c) adsorption energies on N-Ni $_3S_2$ and Ni_3S_2 . (d) Calculated hydrogen adsorption free energy on pristine and Mo-doped CoP. (e) Calculated OER steps on pristine and Mo-doped β -CoOOH. (a-c) Reproduced from ref. 141. Copyright 2017 John Wiley θ Sons, Inc. (d and e) Reproduced from ref. 111. Copyright 2018 Elsevier.

(Fig. 13).100 The post characterization of CoSn₂ revealed that the OER process in alkaline media leached a large amount of Sn from the CoSn₂ crystal lattices and simultaneously oxidized Co to CoO_r/CoOOH as an active species. In contrast, during electrocatalytic HERs, only a slight loss of Sn from the surface occurs, exposing the active Co⁰ to protons. The co-existence of Co (as a catalytically active center) and Sn (as a superior electrical conductor) in CoSn₂ nanocrystals led to highly efficient catalytic performance and long-term stability.

2.8 Carbon-based metal-free catalysts

Because of their low cost, mechanical/chemical stability, and structural flexibility, carbon-based metal-free materials have been developed as efficient electrocatalysts for overall water splitting. 101-103 To improve the catalytic activity, co-doping with other elements such as N, S, and P by bottom-up annealing or post treatments methods have been reported. 104,105 For instance, Dai et al. prepared two-dimensional N, S co-doped graphitic sheets (SHG) with a unique hierarchical structure (Fig. 14a and b). 106 The two-electrode water splitting polarization of the SHGbased cell showed a potential of 1.70 V to deliver 10 mA cm⁻² at the initial stage, followed by a stable ≈ 1.68 V for continuous operation (Fig. 14c). After the long-term operation over 19 h, the catalytic behaviors of SHG-based cell outperformed the Pt/RuO₂ combination (Fig. 14d). The outstanding catalytic performance of SHG was rationalized by its unique architecture with a large surface area, rich active sites, and good electron/electrolyte transport properties.

3. Designing strategies

Based on the above-mentioned achievements for efficient bifunctional water splitting, a variety of designing strategies have been employed for improving the activity of electrocatalysts. Herein, we divide the reported designing strategies into several categories, including anion/cation regulation, carbon incorporation or encapsulation, introducing defects and vacancies, and interfacing engineering. In this section, we highlight the rational designing of these strategies with representing typical examples.

Anion/cation regulation

Anion/cation regulation has been considered as a promising strategy to modify the electronic structure and catalytic activity of water splitting electrocatalysts by enhancing the free carrier density and increasing the active sites.107-110 As shown in Fig. 15a, Wu and co-workers synthesized a N-anion-decorated Ni₃S₂ catalyst by a one-step calcination method for bifunctional water splitting.141 A notably low cell voltage of 1.48 V was achieved to deliver 10 mA cm⁻² in an overall water-splitting device by using N-Ni₃S₂ as an electrocatalyst. N anions regulated the morphology and electronic structure of Ni₃S₂ and afforded the optimized Gibbs free-energy (ΔG_{H^*}) for HERs (Fig. 15b) and water adsorption energy ($\Delta G_{H,O^*}$) for OERs (Fig. 15c).

In addition to anion modulation, metal cation doping has also been intensively investigated to explore high-performance electrocatalysts.111-113 For instance, the Mo dopants in CoP catalyst decreased ΔG_{H^*} for HERs (Fig. 15d),¹¹¹ and reduced the energy barrier in a rate-limiting step for OERs (Fig. 15e). The Mo-doped CoP catalyst exhibited a low cell voltage of 1.56 V to generate 10 mA cm⁻² for overall water splitting, outperforming the Pt/C-Ir/C cell.

3.2 Carbon incorporation or encapsulation

The unique structure and intrinsic properties of nanocarbon substrates such as high conductivity, high surface area, and high chemical stability make them attractive for developing efficient electrocatalysts. 114,115 In the past few years, many kinds of electrocatalysts consisting of nanocarbon substrates such as graphenes and carbon nanotubes have been reported for overall water splitting. In 2013, Loh et al. prepared a graphene oxide and copper-centered metal organic framework electrocatalyst, showing an enhanced electrocatalytic properties and stability for both HERs and OERs.116

Doping nanocarbon substrates with other elements such as N, P, S, and B could improve the synergistic effect between active sites and carbon substrates providing an effective way to explore high-performance electrocatalysts. 117-120 For instance, Wang and co-workers reported cobalt-cobalt oxide/N-doped carbon (CoO_x@CN) electrocatalysts by a one-pot thermal treatment method (Fig. 16a and b).121 Benefiting from the high conductivity of carbon and the synergistic effect of metallic cobalt/cobalt oxide, CoO_x@CN hybrids exhibited remarkable overall water splitting performance with a cell voltage of 1.55 V at 20 mA cm $^{-2}$. As illustrated in Fig. 17a and b, Zhang et al. fabricated N, B-codoped graphitic carbondecorated cobalt hybrid electrocatalysts (Co/NBC) by a simple solvothermal method. 122 In an overall water splitting cell, the optimized Co/NBC-900 hybrid showed outstanding bifunctional electrocatalytic activity and long-term stability (Fig. 17c, a cell voltage of 1.68 V to drive 10 mA cm⁻²). DFT calculations revealed that the synergistic effects between cobalt-cobalt oxide and N, B-codoped carbon substrates optimized the adsorption/desorption energies of hydrogen and oxygen intermediates for HERs and OERs, respectively (Fig. 17d).

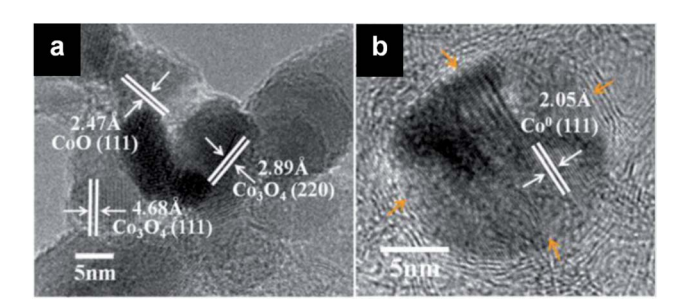


Fig. 16 (a and b) HRTEM images of CoO_x@CN. The brown arrows in (b) point at the graphitic carbon layers. Reproduced from ref. 121. Copyright 2015 American Chemical Society.

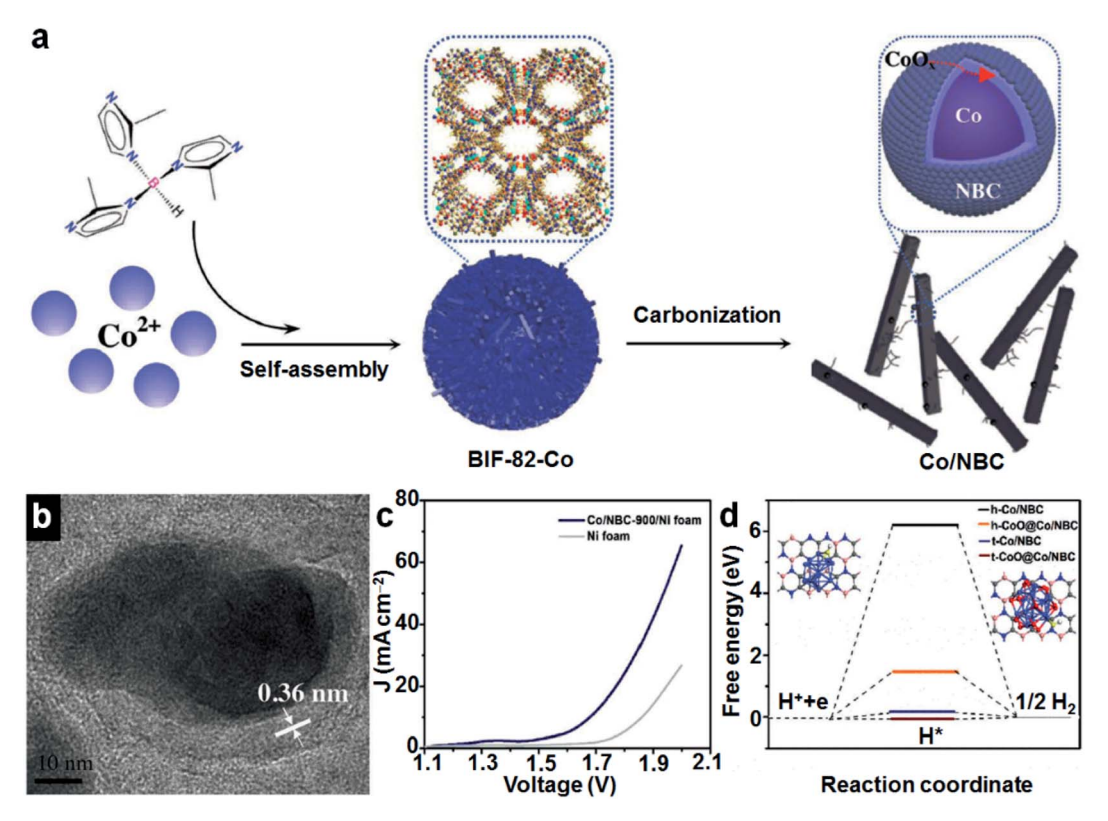


Fig. 17 (a) Schematic of the synthesis of Co/NBC. (b) HRTEM image of Co/NBC-900. (c) LSV curves of overall water splitting in 1.0 M KOH at a scan rate of 5 mV s^{-1} . (d) Calculated hydrogen adsorption free energy on Co/NBC-900 and other control samples. Reproduced from ref. 122. Copyright 2018 John Wiley & Sons, Inc.

3.3 Introduction of defects and vacancies

Defect structures, such as lattice defects, interstitial atoms, and vacancies, widely exist in various nanomaterials.123 Some defects are believed to modify the electronic structures and provide

additional active sites for electrocatalysts. For example, lattice defects in two-dimensional (2D) transition metal-based dichalcogenides expose abundant edge sites for electrocatalysis. 124,125 Another case is that topological defects in nanocarbon substrates are believed to be able to tailor catalytic performances. 123

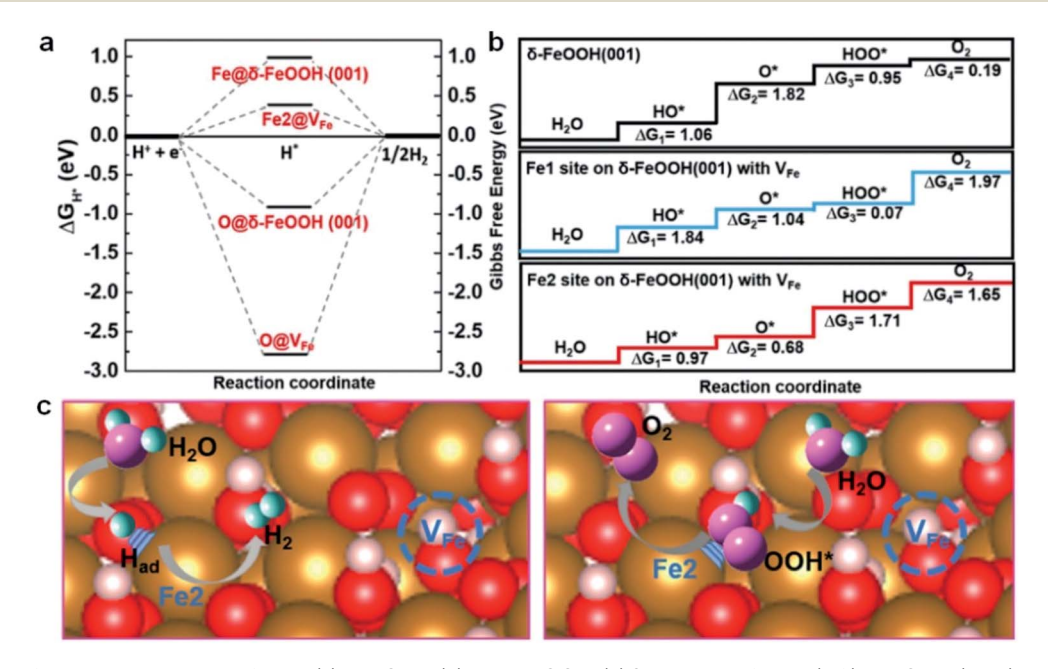


Fig. 18 Calculated free energy diagrams of HERs (a) and OERs (b) on δ -FeOOH. (c) Schematic of HERs (left) and OERs (right) on the Fe2 site of δ -FeOOH with an adjacent iron vacancy (brown: Fe; red: O). Reproduced from ref. 51. Copyright 2018 John Wiley & Sons, Inc.

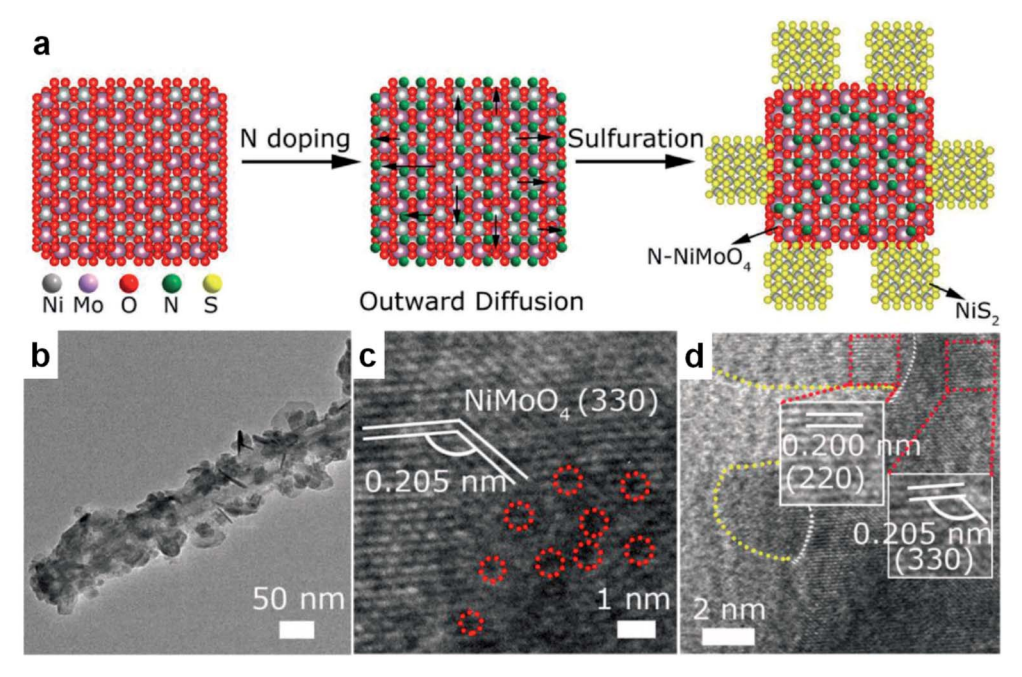


Fig. 19 (a) Schematic of the growth of N-NiMoO₄/NiS₂. (b) TEM and (c and d) HRTEM image of N-NiMoO₄/NiS₂. Reproduced from ref. 132. Copyright 2018 John Wiley & Sons, Inc.

Anion vacancies in transition metal compounds, such as oxygen126 and sulfur vacancies,127 are capable of modulating electronic configuration of catalysts and thus improving the catalytic performances. For instance, O vacancies (V_O) created by plasma in Co₃O₄ were found to be beneficial for its OER activity. 128 More interestingly, Vo could be filled again by P atoms via plasma treatment to enhance its HER activity as well. The filled P atoms significantly modulated the electronic structure of Co₃O₄ and altered binding energies of the reactant intermediates to improve its overall water splitting performance.

Similarly, an alternative option of modifying electrocatalyst is to create metal vacancies, even though this option has been challenged by the high formation energies of most metal vacancies. 123 In order to tackle this issue, a facile wetchemistry method was developed to prepare δ-FeOOH nanosheets with Fe vacancies (VFe).51 Theoretical calculations revealed that V_{Fe} strengthened the binding between H and O (Fig. 18a and c), which adversely weakened the activity on neighboring Fe site (Fe1 site). In contrast, the second Fe atom (Fe2 site) was activated due to the optimized ΔG_{H^*} value. An analogous situation was found for the OER process, wherein it was Fe2, rather than the Fe1 site, that was triggered due to a moderate binding affinity towards the oxygen intermediates (Fig. 18b). Additionally, the electronic conductivity of δ-FeOOH was also improved with the existence of V_{Fe}, which was beneficial for its electrocatalytic performance as well.

3.4 Interfacing engineering

Recent years have witnessed the increasing interest in nano interfaces among heterostructures and hybrid compounds

because of the generated synergetic effects between different moieties to tailor the electronic structures of catalysts. 129 The modulated electronic structure, in turn, influences the overall performance in electrocatalysis. 130 For instance, the interfaces between MoS2 and Ni3S2 facilitated the adsorption of both hydrogen and oxygen intermediates and consequently improved the HER and OER activities of MoS2/Ni3S2 heterostructure.131 It can be rationally anticipated that increasing the number of nano interfaces would enhance the catalytic performances of electrocatalysts, and thus, such a strategy has been increasingly adopted. For example, N integration into a NiMoO4 precursor could increase the interfaces in the final product NiMoO₄/NiS₂ during the sulfurization process. The N dopants was found to promote Ni atoms to diffuse outward and to form epitaxial NiS2 (Fig. 19a), resulting in a unique N-NiMoO₄/NiS₂ nanowire/ nanosheet heterostructure (Fig. 19b). 132 Besides, N dopants also optimized the lattice matching between NiS2 and N-NiMoO₄ by altering the crystal lattice fringes (Fig. 19c) and creating O vacancies, which also increased the number of interfaces (Fig. 19d). Consequently, electrons were transferred from N-NiMoO₄ to NiS₂, optimizing the H adsorption on NiS2 for higher HER activity. This was accompanied by the increased valence state of Ni in N-NiMoO4, resulting in higher OER activities. The N atom itself also optimized the chemical adsorption of both H⁺ and OH⁻ intermediates on NiMoO₄ and the electronic conductivity of the electrocatalyst. As expected, the N-NiMoO₄/NiS₂ catalyst couple required a low cell voltage of only 1.60 V to reach a catalytic current density of 10 mA cm⁻² for overall water splitting electrolysis.

Table 1 Comparison of representative bifunctional electrocatalysts for overall water splitting

Catalyst	Electrolyte	$\eta_{ m HER}$ at j (mV@mA cm $^{-2}$)	HER Tafel slope (mV dec ⁻¹)	$\eta_{ m OER}$ at j (mV@mA cm $^{-2}$)	OER Tafel slope (mV dec ⁻¹)	Overall voltage at j (V@mA cm $^{-2}$)
Phosphides						
Ni_2P^{15}	1.0 M KOH	220@10	_	290@10	47	1.63@10
Co–P film ¹⁴	1.0 M KOH	94@10	42	345@10	47	1.744@100
Ni–P film ¹³⁸	1.0 M KOH	93@10	43	344@10	49	1.67@10
Cu_3P^{12}	0.1 M KOH	222@10	148	412@50	63	_
MoP/NF ¹³⁹	1.0 M KOH	114@10	54.6	265@10	56.6	1.62@10
Ni ₁ Mo ₁ P NSs@MCNTs ¹⁶	1.0 M KOH	135@10	137.5	255@10	45.1	1.601@10
NiCoP/rGO ²²	1.0 M KOH	209@10	124.1	270@10	65.7	1.59@10
Mo-CoP ¹¹¹		_		_		_
Co-P/NC ¹⁴⁰	1.0 M KOH	13@10	65	305@10	56	1.56@10
CO-P/NC	1.0 M KOH	154@10	51	319@10	52	2.0@165
Chalcogenides						
$h-NiS_x^{25}$	1.0 M KOH	60@10	99	180@10	96	1.47@10
FeS/IF ²⁸	1.0 M KOH	300@100	77	238@10	82.7	1.65@10
$Ni_xCo_{3-x}S_4/Ni_3S_2/NF^{30}$	1.0 M KOH	500@719	107	160@10	95	1.58@10
Ni_3S_2/NF^{35}	1.0 M KOH	223@10	_	260@10	_	_
N-Ni ₃ S ₂ /NF ¹⁴¹	1.0 M KOH	110@10	_	350@170	70	1.48@10
MoS_2/Ni_3S_2 (ref. 131)	1.0 M KOH	110@10	83	218@10	88	1.56@10
Co ₃ Se ₄ (ref. 31)	1.0 M KOH	_	_	397@320	44	1.59@10
NiSe/NF ³²	1.0 M KOH	96@10	120	270@20	64	1.63@10
NiSe-NiO _x 142	1.0 M KOH	160@10	—	243@10	128	1.68@10
NISC-NIO _X	1.0 W KOII	100@10		243@10	120	1.08@10
Oxides						
NiFeO _x /CFP ⁴⁰	1.0 M KOH	88@10	_	250@10	31.5	1.51@10
VOOH ⁵⁰	1.0 M KOH	164@10	104	270@10	68	1.62@10
δ-FeOOH NSs/NF ⁵¹	1.0 M KOH	108@10	68	265@10	36	1.62@10
NiFe LDH/Ni foam ⁵²	1.0 M NaOH	210@10	_	240@10	_	1.7@10
FePO ₄ /NF ⁵³	1.0 M KOH	123@10	104.5	218@10	42.7	1.54@10
Co–Mn carbonate hydroxide ⁵⁴	1.0 M KOH	180@10	_	294@30	_	1.68@10
Ni ₁₁ (HPO ₃) ₈ (OH) ₆ (ref. 58)	1.0 M KOH	42@10	102	232@10	91	1.6@10
$SrCo_{0.85}Fe_{0.1}P_{0.05}O_{3-\delta}^{45}$	1.0 M KOH	110@10	94	310@10	55	1.52@10
art. 13						
Nitrides Co ₄ N-VN _{1-x} O _x /CC ⁶⁵	1.0 M KOH	118@10	73.6	262@10	64.1	1.64@10
$CO_4N-VN_{1-x}O_x/CC$		_		263@10		1.64@10
TiN@Ni ₃ N ⁶⁸	1.0 M KOH	21@10	42.1	350@10	93.7	1.64@10
Ni ₃ FeN/r-GO-20 (ref. 70)	1.0 M KOH	213@10	90	270@10	54	1.60@10
Ni-Fe-MoN NTs ⁷¹	1.0 M KOH	55@10	109	228@10	41	1.513@10
Carbides						
Mo ₂ C@CS ⁸⁷	1.0 M KOH	178@10	82	320@10	98	1.73@10
Co_4Mo_2 @NC/ Ti^{143}	1.0 M KOH	218@10	73.5	330@10	48.7	1.74@10
Borides						
FeB ₂ (ref. 91)	1.0 M KOH	61@10	87.5	296@10	52.4	1.57@10
2 ()						
Alloys						
Fe-Co composite films ⁹⁹	1.0 M KOH	163@10	51	283@10	34	1.68@10
CoSn ₂ (ref. 100)	1.0 M KOH	103@10	78	230@10	89	1.55@10
Non-metal catalysts						
N,S-doped graphitic sheets ¹⁰⁶	0.1 M KOH	310@10	112	330@10	71	1.68@10
N/P/F tri-doped graphene ¹⁴⁴	0.1 M KOH	520@10	—	390@10	136	_
Other catalysts	10 14 12011	222@10	115	260@10		1.55@10
$CoO_x@CN^{121}$	1.0 M KOH	232@10	115	260@10	_	1.55@10
NiFe-MOF ¹⁴⁵	0.1 M KOH	134@10		240@10	34	1.55@10
Co/NBC-900 (ref. 122)	1.0 M KOH	117@10	146	302@10	70	1.68@10
	1.0 M KOH	120@10	52	280@10	51.6	1.76@50
P-Co ₃ O ₄ (ref. 128) N-NiMoO ₄ /NiS ₂ (ref. 132)	1.0 M KOH	120@10	74.2	200@10	31.0	1.70@00

Conclusions and outlook

Owing to the growing interest in exploring renewable and sustainable energy resources, developing bifunctional electrocatalysts for overall water splitting may bring an effective method in producing clean hydrogen for the future energy portfolio. This minireview showcased the recent progress in developing nonprecious and bifunctional electrocatalysts for overall water splitting under alkaline conditions, including transition metal-based phosphides, chalcogenides, oxides, nitrides, carbides, borides, alloys, as well as metal-free catalysts. All the representative works discussed herein are compiled in Table 1. Besides, some modification strategies in improving HER and OER performances such as heteroatom modification, carbon incorporation, defect creation, and interfacing engineering were introduced and discussed.

Despite the above-mentioned exciting achievements, there still exists a large space for further improvement as well as some unresolved issues. First, the mechanistic understanding of each step in water splitting electrolysis necessitates in-depth characterization and investigation. In fact, structural changes and true active sites during HERs and OERs at high pH values still remain ambiguous, as redox prefeatures are often observed. Therefore, in situ spectroscopic studies are highly recommended to provide direct evidence regarding the operating mechanisms of water splitting utilizing bifunctional electrocatalysts, which, in turn, is believed to guide the rational design of new electrocatalysts. 133 Second, the design strategy for competent bifunctional electrocatalysts requires further improvement. The nature of two distinctive active sites for the two half redox reactions (HERs and OERs) of water splitting makes it challenging to design a single electrocatalyst active for both reactions. Most of the prevalent modification strategies are limited to a narrow range of materials, whereas a universal strategy applicable for various compositions is highly preferred. Especially for practical applications at an industrial scale, wellcontrolled, low-cost and environmentally friendly synthesis is desirable. In addition to catalytic bifunctionality, the sufficient long-term stability of electrocatalysts operating at large current density $(e.g., 1 \text{ A cm}^{-2})$ is another critical factor for commercial electrolyzers, which have received much less attention till today. It requires not only high corrosion tolerance under extreme conditions but also robust adhesion to current collectors. At present, only self-supported catalysts have demonstrated the catalytic performance at large current density, such as Ni foamor Fe foam-based transition metal-based catalysts. 134,135 Third, the development of bifunctional electrocatalysts functioning in a wide pH range is still in the infancy stage. It is mainly restricted by the poor tolerance of most 1st-row transition metal-based OER electrocatalysts in low pH electrolytes. Even though neutral pH electrolytes bear the best environmental friendliness, most electrocatalysts exhibit mediocre efficiency for both HERs and OERs at pH 7, probably due to the low conductivity of neutral electrolytes. Although a few examples of low-cost electrocatalysts have been reported with performances superior to those of noble metal-based counterparts, 136,137 most

bifunctional electrocatalysts cannot compete the integrated noble metal-based electrocatalyst couples for overall water splitting. We hope this review will bring useful guidance and motivation to our peers in developing innovative and competent bifunctional electrocatalysts for hydrogen production from water splitting electrolysis.

Conflicts of interest

There are no conflicts to declare.

Acknowledgements

Y. S. acknowledges the financial support of the Herman Frasch Foundation (820-HF17), National Science Foundation (CHE-1914546), and the University of Cincinnati.

References

- 1 J. M. Bockris and E. C. Potter, J. Electrochem. Soc., 1952, 99, 169-186.
- 2 L. Zhang, J. Xiao, H. Wang and M. Shao, ACS Catal., 2017, 7, 7855-7865.
- 3 T. Bak, J. Nowotny, M. Rekas and C. Sorrell, Int. J. Hydrogen Energy, 2002, 27, 991-1022.
- 4 C. Tang, H.-F. Wang and Q. Zhang, Acc. Chem. Res., 2018, 51, 881-889.
- 5 Y. Shi and B. Zhang, Chem. Soc. Rev., 2016, 45, 1529-1541.
- 6 S. Carenco, D. Portehault, C. Boissiere, N. Mezailles and C. Sanchez, Chem. Rev., 2013, 113, 7981-8065.
- 7 P. Liu and J. A. Rodriguez, J. Am. Chem. Soc., 2005, 127, 14871-14878.
- 8 E. J. Popczun, J. R. McKone, C. G. Read, A. J. Biacchi, A. M. Wiltrout, N. S. Lewis and R. E. Schaak, J. Am. Chem. Soc., 2013, 135, 9267-9270.
- 9 E. J. Popczun, C. G. Read, C. W. Roske, N. S. Lewis and R. E. Schaak, Angew. Chem., Int. Ed., 2014, 53, 5427-5430.
- 10 P. Jiang, Q. Liu, Y. Liang, J. Tian, A. M. Asiri and X. Sun, Angew. Chem., Int. Ed., 2014, 53, 12855-12859.
- 11 J. F. Callejas, J. M. McEnaney, C. G. Read, J. C. Crompton, A. J. Biacchi, E. J. Popczun, T. R. Gordon, N. S. Lewis and R. E. Schaak, ACS Nano, 2014, 8, 11101-11107.
- 12 J. Tian, Q. Liu, N. Cheng, A. M. Asiri and X. Sun, Angew. Chem., Int. Ed., 2014, 53, 9577-9581.
- 13 Z. Y. Zhang, S. S. Liu, J. Xiao and S. Wang, J. Mater. Chem. A, 2016, 4, 9691-9699.
- 14 N. Jiang, B. You, M. Sheng and Y. Sun, Angew. Chem., Int. Ed., 2015, 54, 6251-6254.
- 15 L.-A. Stern, L. Feng, F. Song and X. Hu, Energy Environ. Sci., 2015, 8, 2347-2351.
- 16 H. Xu, J. Wei, K. Zhang, Y. Shiraishi and Y. Du, ACS Appl. Mater. Interfaces, 2018, 10, 29647-29655.
- 17 Z. Zhao, D. E. Schipper, A. P. Leitner, H. Thirumalai, J.-H. Chen, L. Xie, F. Qin, M. K. Alam, L. C. Grabow and S. Chen, Nano Energy, 2017, 39, 444-453.

- 18 H. Liang, A. N. Gandi, D. H. Anjum, X. Wang, U. Schwingenschlögl and H. N. Alshareef, *Nano Lett.*, 2016, 16, 7718–7725.
- 19 J. Gao, L. Yang, D. Wang and D. P. Cao, *Chem.-Eur. J.*, 2020, **26**, 4112–4119.
- 20 Y. T. Yan, J. H. Lin, J. Cao, S. Guo, X. H. Zheng, J. C. Feng and J. L. Qi, *J. Mater. Chem. A*, 2019, 7, 24486–24492.
- 21 M. Q. Yao, H. H. Hu, B. L. Sun, N. Wang, W. C. Hu and S. Komarneni, *Small*, 2019, 15, 1905201.
- 22 J. Li, M. Yan, X. Zhou, Z. Q. Huang, Z. Xia, C. R. Chang, Y. Ma and Y. Qu, *Adv. Funct. Mater.*, 2016, **26**, 6785–6796.
- 23 X. Ma, Y. Chang, Z. Zhang and J. Tang, *J. Mater. Chem. A*, 2018, **6**, 2100–2106.
- 24 J. D. Benck, T. R. Hellstern, J. Kibsgaard, P. Chakthranont and T. F. Jaramillo, *ACS Catal.*, 2014, 4, 3957–3971.
- 25 B. You and Y. Sun, Adv. Energy Mater., 2016, 6, 1502333.
- 26 J. Dong, F.-Q. Zhang, Y. Yang, Y.-B. Zhang, H. He, X. Huang, X. Fan and X.-M. Zhang, *Appl. Catal.*, B, 2018, 243, 693–702.
- 27 J. Wang, H.-x. Zhong, Z.-l. Wang, F.-l. Meng and X.-b. Zhang, ACS Nano, 2016, 10, 2342.
- 28 X. Zou, Y. Wu, Y. Liu, D. Liu, W. Li, L. Gu, H. Liu, P. Wang, L. Sun and Y. Zhang, *Chem*, 2018, 4, 1139–1152.
- 29 J. Yu, G. Cheng and W. Luo, *J. Mater. Chem. A*, 2017, 5, 15838–15844.
- 30 Y. Wu, Y. Liu, G.-D. Li, X. Zou, X. Lian, D. Wang, L. Sun, T. Asefa and X. Zou, *Nano Energy*, 2017, 35, 161–170.
- 31 W. Li, X. Gao, D. Xiong, F. Wei, W. G. Song, J. Xu and L. Liu, *Adv. Energy Mater.*, 2017, 7, 1602579.
- 32 C. Tang, N. Cheng, Z. Pu, W. Xing and X. Sun, *Angew. Chem.*, *Int. Ed.*, 2015, **54**, 9351–9355.
- 33 R. Xu, R. Wu, Y. Shi, J. Zhang and B. Zhang, *Nano Energy*, 2016, 24, 103–110.
- 34 C. Panda, P. W. Menezes, C. Walter, S. Yao, M. E. Miehlich, V. Gutkin, K. Meyer and M. Driess, *Angew. Chem., Int. Ed.*, 2017, 56, 10506–10510.
- 35 L.-L. Feng, G. Yu, Y. Wu, G.-D. Li, H. Li, Y. Sun, T. Asefa, W. Chen and X. Zou, *J. Am. Chem. Soc.*, 2015, 137, 14023– 14026.
- 36 C. Panda, P. W. Menezes, C. Walter, S. Yao, M. E. Miehlich, V. Gutkin, K. Meyer and M. Driess, Angew. Chem., Int. Ed., 2017, 56, 10506–10510.
- 37 H. Jin, C. Guo, X. Liu, J. Liu, A. Vasileff, Y. Jiao, Y. Zheng and S.-Z. Qiao, *Chem. Rev.*, 2018, **118**, 6337–6408.
- 38 M. W. Kanan, Y. Surendranath and D. G. Nocera, *Chem. Soc. Rev.*, 2009, **38**, 109–114.
- 39 Z. Y. Zhang, S. S. Liu, F. Xiao and S. Wang, *ACS Sustainable Chem. Eng.*, 2017, 5, 529–536.
- 40 H. Wang, H. W. Lee, Y. Deng, Z. Lu, P. C. Hsu, Y. Liu, D. Lin and Y. Cui, *Nat. Commun.*, 2015, **6**, 7261.
- 41 A. Kojima, K. Teshima, Y. Shirai and T. Miyasaka, *J. Am. Chem. Soc.*, 2009, **131**, 6050–6051.
- 42 D. Chen, C. Chen, Z. M. Baiyee, Z. Shao and F. Ciucci, *Chem. Rev.*, 2015, **115**, 9869–9921.
- 43 J. Suntivich, K. J. May, H. A. Gasteiger, J. B. Goodenough and Y. Shao-Horn, *Science*, 2011, 334, 1383–1385.
- 44 J. Wang, Y. Gao, D. Chen, J. Liu, Z. Zhang, Z. Shao and F. Ciucci, *ACS Catal.*, 2017, **8**, 364–371.

- 45 G. Chen, Z. Hu, Y. Zhu, B. Gu, Y. Zhong, H. J. Lin, C. T. Chen, W. Zhou and Z. Shao, *Adv. Mater.*, 2018, 30, 1804333.
- 46 Y. Zhu, W. Zhou, Y. Zhong, Y. Bu, X. Chen, Q. Zhong, M. Liu and Z. Shao, *Adv. Energy Mater.*, 2017, 7, 1602122.
- 47 H. Yin and Z. Tang, Chem. Soc. Rev., 2016, 45, 4873-4891.
- 48 H. Jin, C. Guo, X. Liu, J. Liu, A. Vasileff, Y. Jiao, Y. Zheng and S.-Z. Qiao, *Chem. Rev.*, 2018, **118**, 6337–6408.
- 49 Z. Xing, L. Gan, J. Wang and X. Yang, *J. Mater. Chem. A*, 2017, 5, 7744–7748.
- 50 H. Shi, H. Liang, F. Ming and Z. Wang, *Angew. Chem., Int. Ed.*, 2017, **56**, 573–577.
- 51 B. Liu, Y. Wang, H. Q. Peng, R. Yang, Z. Jiang, X. Zhou, C. S. Lee, H. Zhao and W. Zhang, *Adv. Mater.*, 2018, 30, 1803144.
- 52 J. Luo, J.-H. Im, M. T. Mayer, M. Schreier, M. K. Nazeeruddin, N.-G. Park, S. D. Tilley, H. J. Fan and M. Grätzel, Science, 2014, 345, 1593–1596.
- 53 L. Yang, Z. Guo, J. Huang, Y. Xi, R. Gao, G. Su, W. Wang, L. Cao and B. Dong, *Adv. Mater.*, 2017, 29, 1704574.
- 54 T. Tang, W.-J. Jiang, S. Niu, N. Liu, H. Luo, Y.-Y. Chen, S.-F. Jin, F. Gao, L.-J. Wan and J.-S. Hu, *J. Am. Chem. Soc.*, 2017, **139**, 8320–8328.
- 55 L. Hui, Y. Xue, D. Jia, H. Yu, C. Zhang and Y. Li, Adv. Energy Mater., 2018, 8, 1800175.
- 56 S. Jin, ACS Energy Lett., 2017, 2, 1937-1938.
- 57 R. Subbaraman, D. Tripkovic, D. Strmenik, K.-C. Chang, M. Uchimura, A. P. Paulikas, V. Stamenkovic and N. M. Markovic, *Science*, 2011, 334, 1256–1260.
- 58 P. W. Menezes, C. Panda, S. Loos, F. Bunschei-Bruns, C. Walter, M. Schwarze, X. Deng, H. Dau and M. Driess, *Energy Environ. Sci.*, 2018, 11, 1287–1298.
- 59 N. Han, P. Liu, J. Jiang, L. Ai, Z. Shao and S. Liu, J. Mater. Chem. A, 2018, 6, 19912–19933.
- 60 S. Dong, X. Chen, X. Zhang and G. Cui, Coord. Chem. Rev., 2013, 257, 1946–1956.
- 61 J. Xiong, W. Cai, W. Shi, X. Zhang, J. Li, Z. Yang, L. Feng and H. Cheng, *J. Mater. Chem. A*, 2017, 5, 24193–24198.
- 62 J. Song, G. Li, F. Xiong and X. Gao, *J. Mater. Chem.*, 2012, 22, 20580–20585.
- 63 Z.-Y. Wu, W.-B. Ji, B.-C. Hu, H.-W. Liang, X.-X. Xu, Z.-L. Yu, B.-Y. Li and S.-H. Yu, *Nano Energy*, 2018, **51**, 286–293.
- 64 M. Shalom, D. Ressnig, X. Yang, G. Clavel, T. P. Fellinger and M. Antonietti, *J. Mater. Chem. A*, 2015, 3, 8171–8177.
- 65 S. Dutta, A. Indra, Y. Feng, H. Han and T. Song, *Appl. Catal.*, *B*, 2019, **241**, 521–527.
- 66 F.-C. Shen, S.-N. Sun, Z.-F. Xin, S.-L. Li, L.-Z. Dong, Q. Huang, Y.-R. Wang, J. Liu and Y.-Q. Lan, *Appl. Catal.*, B, 2019, 243, 470–480.
- 67 A. Wu, Y. Xie, H. Ma, C. Tian, Y. Gu, H. Yan, X. Zhang, G. Yang and H. Fu, *Nano Energy*, 2018, 44, 353–363.
- 68 Q. Zhang, Y. Wang, Y. Wang, A. M. Al-Enizi, A. A. Elzatahry and G. Zheng, *J. Mater. Chem. A*, 2016, 4, 5713–5718.
- 69 B. Zhang, C. Xiao, S. Xie, J. Liang, X. Chen and Y. Tang, Chem. Mater., 2016, 28, 6934–6941.
- 70 Y. Gu, S. Chen, J. Ren, Y. A. Jia, C. Chen, S. Komarneni, D. Yang and X. Yao, ACS Nano, 2018, 12, 245–253.

- 71 C. Zhu, Z. Yin, W. Lai, Y. Sun, L. Liu, X. Zhang, Y. Chen and S. L. Chou, Adv. Energy Mater., 2018, 1802327.
- 72 C. Wan, Y. N. Regmi and B. M. Leonard, Angew. Chem., Int. Ed., 2014, 53, 6407-6410.
- 73 J. Zhu, K. Sakaushi, G. Clavel, M. Shalom, M. Antonietti and T.-P. Fellinger, J. Am. Chem. Soc., 2015, 137, 5480-5485.
- 74 W.-F. Chen, C.-H. Wang, K. Sasaki, N. Marinkovic, W. Xu, J. Muckerman, Y. Zhu and R. Adzic, Energy Environ. Sci., 2013, 6, 943-951.
- 75 Y. Liu, G. Yu, G. D. Li, Y. Sun, T. Asefa, W. Chen and X. Zou, Angew. Chem., Int. Ed., 2015, 54, 10752-10757.
- 76 Y. N. Regmi, G. R. Waetzig, K. D. Duffee, S. M. Schmuecker, J. M. Thode and B. M. Leonard, J. Mater. Chem. A, 2015, 3, 10085-10091.
- 77 Y. Zhao, K. Kamiya, K. Hashimoto and S. Nakanishi, Angew. Chem., Int. Ed., 2013, 52, 13638-13641.
- 78 D. V. Esposito, S. T. Hunt, Y. C. Kimmel and J. G. Chen, J. Am. Chem. Soc., 2012, 134, 3025-3033.
- 79 L. Ma, S. Sui and Y. Zhai, J. Power Sources, 2008, 177, 470-477
- 80 F. Kong, X. Fan, A. Kong, Z. Zhou, X. Zhang and Y. Shan, Adv. Funct. Mater., 2018, 1803973.
- 81 H. Yang, S. Luo, X. Li, S. Li, J. Jin and J. Ma, J. Mater. Chem. A, 2016, 4, 18499-18508.
- 82 Z. Kou, L. Zhang, Y. Ma, X. Liu, W. Zang, J. Zhang, S. Huang, Y. Du, A. K. Cheetham and J. Wang, Appl. Catal., B, 2019, 243, 678-685.
- 83 B. Maribo-Mogensen, G. M. Kontogeorgis and K. Thomsen, J. Phys. Chem. B, 2013, 117, 3389-3397.
- 84 C. A. Wolden, A. Pickerell, T. Gawai, S. Parks, J. Hensley and J. D. Way, ACS Appl. Mater. Interfaces, 2011, 3, 517-521.
- 85 S. Chouzier, T. Czeri, M. Roy-Auberger, C. Pichon, C. Geantet, M. Vrinat and P. Afanasiev, J. Solid State Chem., 2011, 184, 2668-2677.
- 86 H.-M. Wang, X.-H. Wang, M.-H. Zhang, X.-Y. Du, W. Li and K.-Y. Tao, Chem. Mater., 2007, 19, 1801-1807.
- 87 H. Wang, Y. Cao, C. Sun, G. Zou, J. Huang, X. Kuai, J. Zhao and L. Gao, ChemSusChem, 2017, 10, 3540-3546.
- 88 Q. Hu, X. Liu, B. Zhu, L. Fan, X. Chai, Q. Zhang, J. Liu, C. He and Z. Lin, Nano Energy, 2018, 50, 212-219.
- 89 H. Chen and X. X. Zou, Inorg. Chem. Front., 2020, DOI: 10.1039/D0QI00146E.
- 90 J. Masa, P. Weide, D. Peeters, I. Sinev, W. Xia, Z. Sun, C. Somsen, M. Muhler and W. Schuhmann, Adv. Energy Mater., 2016, 6, 1502313.
- 91 H. Li, P. Wen, Q. Li, C. Dun, J. Xing, C. Lu, S. Adhikari, L. Jiang, D. L. Carrol and S. M. Geyer, Adv. Energy Mater., 2017, 7, 1700513.
- 92 H. Vrubel and X. Hu, Angew. Chem., Int. Ed., 2012, 51, 12703-12706.
- 93 J. M. V. Nsanzimana, V. Reddu, Y. Peng, Z. Huang, C. Wang and X. Wang, Chem.-Eur. J., 2018, 24, 18502-18511.
- 94 Y. Chen, G. Yu, W. Chen, Y. Liu, G.-D. Li, P. Zhu, Q. Tao, Q. Li, J. Liu and X. Shen, J. Am. Chem. Soc., 2017, 139, 12370-12373.
- 95 T. Osaka, H. Ishibashi, T. Endo and T. Yoshida, Electrochim. Acta, 1981, 26, 339-343.

- 96 R. Cava, H. Takagi, H. Zandbergen, J. Krajewski, W. Peck Jr, T. Siegrist, B. Batlogg, R. Van Dover, R. Felder and K. Mizuhashi, Nature, 1994, 367, 252-253.
- 97 M. Armbrüster, R. Schlögl and Y. Grin, Sci. Technol. Adv. Mater., 2014, 15, 034803.
- 98 X. Wang, X. Liu, C.-J. Tong, X. Yuan, W. Dong, T. Lin, L.-M. Liu and F. Huang, J. Mater. Chem. A, 2016, 4, 7762-7771.
- 99 W. Liu, K. Du, L. Liu, J. Zhang, Z. Zhu, Y. Shao and M. Li, Nano Energy, 2017, 38, 576-584.
- 100 P. W. Menezes, C. Panda, S. Garai, C. Walter, A. Guiet and M. Driess, Angew. Chem., Int. Ed., 2018, 57, 15237-15242.
- 101 D. S. Su, S. Perathoner and G. Centi, *Chem. Rev.*, 2013, 113, 5782-5816.
- 102 B. Xiong, L. Chen and J. Shi, ACS Catal., 2018, 8, 3688-3707.
- 103 L. Zhang, J. Xiao, H. Wang and M. Shao, ACS Catal., 2017, 7, 7855-7865.
- 104 J. Zhang, L. Qu, G. Shi, J. Liu, J. Chen and L. Dai, Angew. Chem., Int. Ed., 2016, 55, 2230-2234.
- 105 Z. Y. Zhang, Z. R. Yi, J. Wang, X. Tian, P. Xu, G. Q. Shi and S. Wang, J. Mater. Chem. A, 2017, 5, 17064-17072.
- 106 C. Hu and L. Dai, Adv. Mater., 2017, 29, 1604942.
- 107 M. S. Faber, M. A. Lukowski, Q. Ding, N. S. Kaiser and S. Jin, J. Phys. Chem. C, 2014, 118, 21347-21356.
- 108 D. Kong, J. J. Cha, H. Wang, H. R. Lee and Y. Cui, Energy Environ. Sci., 2013, 6, 3553-3558.
- 109 Q. Liu, J. Tian, W. Cui, P. Jiang, N. Cheng, A. M. Asiri and X. Sun, Angew. Chem., Int. Ed., 2014, 53, 6710-6714.
- 110 T. Liu, X. Ma, D. Liu, S. Hao, G. Du, Y. Ma, A. M. Asiri, X. Sun and L. Chen, ACS Catal., 2016, 7, 98-102.
- 111 C. Guan, W. Xiao, H. Wu, X. Liu, W. Zang, H. Zhang, J. Ding, Y. P. Feng, S. J. Pennycook and J. Wang, Nano Energy, 2018, 48, 73-80.
- 112 C. Tang, R. Zhang, W. Lu, L. He, X. Jiang, A. M. Asiri and X. Sun, Adv. Mater., 2017, 29, 1602441.
- 113 T. Liu, D. Liu, F. Qu, D. Wang, L. Zhang, R. Ge, S. Hao, Y. Ma, G. Du and A. M. Asiri, Adv. Energy Mater., 2017, 7, 1700020.
- 114 Y. P. Zhu, C. Guo, Y. Zheng and S.-Z. Qiao, Acc. Chem. Res., 2017, 50, 915-923.
- 115 Y. Yu, Y. Shi and B. Zhang, Acc. Chem. Res., 2018, 51, 1711-
- 116 M. Jahan, Z. Liu and K. P. Loh, Adv. Funct. Mater., 2013, 23, 5363-5372.
- 117 J. Deng, P. Ren, D. Deng and X. Bao, Angew. Chem., Int. Ed., 2015, 54, 2100-2104.
- 118 M. Tavakkoli, T. Kallio, O. Reynaud, A. G. Nasibulin, C. Johans, J. Sainio, H. Jiang, E. I. Kauppinen and K. Laasonen, Angew. Chem., Int. Ed., 2015, 54, 4535-4538.
- 119 S. Wang, J. Wang, M. Zhu, X. Bao, B. Xiao, D. Su, H. Li and Y. Wang, J. Am. Chem. Soc., 2015, 137, 15753-15759.
- 120 Y. P. Zhu, C. Guo, Y. Zheng and S.-Z. Qiao, Acc. Chem. Res., 2017, 50, 915-923.
- 121 H. Jin, J. Wang, D. Su, Z. Wei, Z. Pang and Y. Wang, J. Am. Chem. Soc., 2015, 137, 2688-2694.
- 122 M. R. Liu, Q. L. Hong, Q. H. Li, Y. Du, H. X. Zhang, S. Chen, T. Zhou and J. Zhang, Adv. Funct. Mater., 2018, 1801136.

- 123 D. Yan, Y. Li, J. Huo, R. Chen, L. Dai and S. Wang, *Adv. Mater.*, 2017, **29**, 1606459.
- 124 J. Xie, H. Zhang, S. Li, R. Wang, X. Sun, M. Zhou, J. Zhou, X. W. Lou and Y. Xie, *Adv. Mater.*, 2013, 25, 5807–5813.
- 125 H. Wang, X. B. Li, L. Gao, H. L. Wu, J. Yang, L. Cai, T. B. Ma, C. H. Tung, L. Z. Wu and G. Yu, *Angew. Chem., Int. Ed.*, 2018, 57, 192–197.
- 126 L. Zhuang, L. Ge, Y. Yang, M. Li, Y. Jia, X. Yao and Z. Zhu, *Adv. Mater.*, 2017, **29**, 1606793.
- 127 H. Li, C. Tsai, A. L. Koh, L. Cai, A. W. Contryman, A. H. Fragapane, J. Zhao, H. S. Han, H. C. Manoharan and F. Abild-Pedersen, *Nat. Mater.*, 2016, **15**, 48.
- 128 Z. Xiao, Y. Wang, Y.-C. Huang, Z. Wei, C.-L. Dong, J. Ma, S. Shen, Y. Li and S. Wang, *Energy Environ. Sci.*, 2017, **10**, 2563–2569.
- 129 Y. Wang, B. Kong, D. Zhao, H. Wang and C. Selomulya, *Nano Today*, 2017, **15**, 26–55.
- 130 S. Bai, C. Wang, M. Deng, M. Gong, Y. Bai, J. Jiang and Y. Xiong, *Angew. Chem., Int. Ed.*, 2014, 53, 12120–12124.
- 131 J. Zhang, T. Wang, D. Pohl, B. Rellinghaus, R. Dong, S. Liu, X. Zhuang and X. Feng, *Angew. Chem., Int. Ed.*, 2016, 55, 6702–6707.
- 132 L. An, J. Feng, Y. Zhang, R. Wang, H. Liu, G. C. Wang, F. Cheng and P. Xi, *Adv. Funct. Mater.*, 2018, 1805298.
- 133 Y. Jiao, Y. Zheng, M. Jaroniec and S. Z. Qiao, *Chem. Soc. Rev.*, 2015, **44**, 2060–2086.

- 134 Y. Liu, X. Liang, L. Gu, Y. Zhang, G. D. Li, X. X. Zou and J. S. Chen, *Nat. Commun.*, 2018, 9, 2609.
- 135 J. Q. Zhang, X. Shang, H. Ren, J. Q. Chi, H. Fu, B. Dong, C. G. Liu and Y. M. Chai, *Adv. Mater.*, 2019, **31**, 1905107.
- 136 B. You, X. Liu, G. Hu, S. Gul, J. Yano, D.-e. Jiang and Y. Sun, *J. Am. Chem. Soc.*, 2017, **139**, 12283–12290.
- 137 F. Song, W. Li, J. Yang, G. Han, P. Liao and Y. Sun, *Nat. Commun.*, 2018, **9**, 4531.
- 138 N. Jiang, B. You, M. Sheng and Y. Sun, *ChemCatChem*, 2016, **8**, 106–112.
- 139 Y. Jiang, Y. Lu, J. Lin, X. Wang and Z. Shen, *Small Methods*, 2018, 2, 1700369.
- 140 B. You, N. Jiang, M. Sheng, S. Gul, J. Yano and Y. Sun, *Chem. Mater.*, 2015, 27, 7636–7642.
- 141 P. Chen, T. Zhou, M. Zhang, Y. Tong, C. Zhong, N. Zhang, L. Zhang, C. Wu and Y. Xie, Adv. Mater., 2017, 29, 1701584.
- 142 R. Gao, G.-D. Li, J. Hu, Y. Wu, X. Lian, D. Wang and X. Zou, *Catal. Sci. Technol.*, 2016, **6**, 8268–8275.
- 143 J. Jiang, Q. Liu, C. Zeng and L. Ai, *J. Mater. Chem. A*, 2017, 5, 16929–16935.
- 144 J. Zhang and L. Dai, *Angew. Chem., Int. Ed.*, 2016, 55, 13296–13300.
- 145 J. Duan, S. Chen and C. Zhao, Nat. Commun., 2017, 8, 15341.